AN EULERIAN INTERFACE-CAPTURING APPROACH FOR COMPRESSIBLE TWO-PHASE FLOW WITH VAN DER WAALS-TYPE FLUIDS *

KEH-MING SHYUE †

Abstract. Our goal is to present a simple interface-capturing approach to compressible two-phase (liquid-gas) flow problems in two space dimensions. We use the Euler equations of gas dynamics as a model system, and consider problems with the Tait and van der Waals equations of state for describing material property of the liquid and gas, respectively. The algorithm uses a modified van der Waals equation of state as a basis for the liquid-gas coexistent cell, and has a mixture type of the model equations written in quasi-conservative form to ensure the correct fluid mixing when approximating the equations numerically with interfaces. A standard high-resolution method based on a wave-propagation formulation is employed to solve the proposed model system. Several numerical results are presented that show the feasibility of the method to practical problems without any spurious oscillations in the pressure near the interfaces. This includes convergence results of a radially symmetry problem and some tests of a shock wave in bubbly liquids. Extension of the model to cases with source terms is briefly discussed, and a sample accuracy study of a spherically symmetric flow is shown.

Key words. interface capturing method, bubbly liquids, tait equation of state, two-phase flow, van der Waals fluids

AMS subject classifications. 65M06, 76L05, 76M20, 76T05

1. Introduction. This paper is concerned with the development of a simple interface-capturing approach for efficient numerical resolution of compressible two-phase flow with van der Waals-type fluids (*i.e.*, a fluid with the finite size of a molecule and the nonzero cohesive forces between molecules [21]). We consider a simplified model problem in two space dimensions that the fluids of interests consist of two different fluid components: liquid and gas, separated by interfaces, see Fig. 1.1 for a sample two-phase flow setup. In the algorithm, we use an Eulerian formulation of the equations that, on the gas-phase part of the domain, we have

$$\partial_t \begin{bmatrix} \rho \\ \rho u \\ \rho v \\ \rho E \end{bmatrix} + \partial_x \begin{bmatrix} \rho u \\ \rho u^2 + p \\ \rho uv \\ \rho E u + pu \end{bmatrix} + \partial_y \begin{bmatrix} \rho v \\ \rho uv \\ \rho v^2 + p \\ \rho E v + pv \end{bmatrix} = 0, \tag{1.1}$$

where ρ is the density, u and v are the velocities in the x- and y-direction respectively, p is the pressure, and E is the total energy per unit mass. We assume that the gas satisfies a van der Waals equation of state,

$$p(\rho,\varepsilon) = \left(\frac{\gamma - 1}{1-\beta\rho}\right)\rho\varepsilon, \tag{1.2}$$

so as to deal with the possible real-gas effect when both the temperature and pressure are high [21, 66]. Here ε denotes the internal energy per unit mass, γ is the ratio of specific heats ($\gamma > 1$), β is the finite size of molecules constant ($0 \le \beta\rho < 1$) [39], and

*This work was supported in part by National Science Council of Republic of China Grants NSC-86-2115-M-002-005 and NSC-87-2115-M-002-016.

†Department of Mathematics, National Taiwan University, Taipei, Taiwan, 106, Republic of China (`shyue@math.ntu.edu.tw`). Version of November 12, 1998.

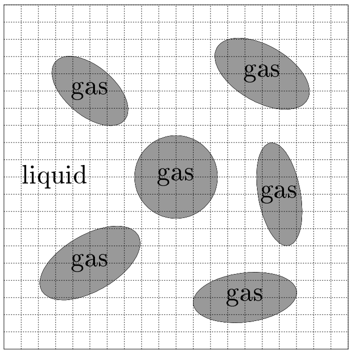

FIG. 1.1. *A typical example of a two-phase flow setup with interfaces that separate regions of two different fluid components: liquid and gas, into two parts. Note it is those grid cells that are cut by the interfaces requiring special attentions for proper numerical treatments.*

as usual $E = \varepsilon + (u^2 + v^2)/2$. Note that the four components of Eqs. (1.1) express the conservation of mass, momenta in the x- and y-direction, and energy, respectively [15].

On the liquid-phase part of the domain, however, the algorithm uses a widely employed Tait equation of state,

$$p(\rho) = \mathcal{A}\rho^{\gamma} - \mathcal{B}, \tag{1.3}$$

for a fundamental characterization of material properties of the liquids. Here $\mathcal{A}$ and $\mathcal{B}$ are nonnegative material-dependent constants that together with γ can be determined by a fitting procedure from laboratory data [69]. Note $\mathcal{B}$ can be viewed as a linear version of the cohesive force term to a more general van der Waals fluid (cf. [21]). Typical set of parameter values are, for water: $\gamma = 7$, $\mathcal{A} = 3001$ atm, $\mathcal{B} = 3000$ atm [15], and for human blood: $\gamma = 5.527$, $\mathcal{A} = 614.6$ MPa, $\mathcal{B} = 614.6$ MPa [42], approximately. It is important to note that because of the solely density-dependence of the pressure p in liquids, see (1.3), the energy equation of the Euler Eqs. (1.1) plays no active role to the description of the flow, and hence can be neglected. For completeness, we write down the equations of motion for a liquid as follows,

$$\partial_t \begin{bmatrix} \rho \\ \rho u \\ \rho v \end{bmatrix} + \partial_x \begin{bmatrix} \rho u \\ \rho u^2 + p(\rho) \\ \rho u v \end{bmatrix} + \partial_y \begin{bmatrix} \rho v \\ \rho u v \\ \rho v^2 + p(\rho) \end{bmatrix} = 0, \tag{1.4}$$

where the pressure p is set by (1.3).

We want to use a state-of-the-art shock-capturing method on a uniform rectangular grid for the two-phase flow computations. Clearly when grid cells contain only a single phase of the fluid, there is no problem in describing the motion of each of the phases individually (cf. Eqs. (1.1)–(1.4) of the current liquid-gas case). But in practice due to the presence and the subsequent dynamic-evolution of the interfaces by the solutions of the governing system, it is inevitable to have grid cells consisting of two or more fluid components within a cell (see Fig. 1.1). Because of this, the need to give a proper modeling and approximation of these *mixture* grid cells becomes a principle issue in many of the multicomponent algorithms developed in the literatures, see [1, 12, 19, 20, 25, 26, 40, 52], for example.

The approach we take here is an extension of the work described by the author [52, 53] in that as opposed to a simplier case with the stiffened gas equation of state, a modified van der Waals equation of state is introduced as a basic element to the current liquid-gas coexistent cell (see Section 2.1). Then, from Eq. (1.1), in particular from the energy equation, conditions for the mixture of the material-dependent constants of the proposed equation of state are derived so that not only the pressure remains in equilibrium near the interfaces, but also the mass preserves its conservation on the whole domain. When combining these conditions to the full Euler Eq. (1.1) gives a quasi-conservative system of equations that is valid for the fluid-mixture cells on the macroscopic level. A complete two-phase flow model is formed then by the inclusion of an evolution equation based on a volume-fraction formulation of the interface capturing (see Section 2.2). Numerical results to be presented in Section 4 show that this is a viable approach to practical problems without any spurious oscillations in the pressure near the interfaces when approximating the model equations in a consistent manner by a high-resolution wave propagation method [28, 33, 38]. This will be discussed further in Section 3.

It is true that in many two-phase flow applications physical effects, such as surface tension and viscosity, play an important role to the dynamics of the interfaces, and thus should be included to the model for realization. Typical examples of this kind are the popular water-drop problem in air and the rising air bubble problem in water. In these instances, because the fluids are mostly in a low Mach number regime, compressibility of the fluids is often ignored, and so the problem is formulated into an incompressible form (cf. [8, 56, 57, 62]).

Here in contrast to the work just mentioned, we consider a class of problems where the influence of compressibility of the fluids to the solutions is vital, but not the surface tension and viscosity. Examples cover a family of shock wave problems with interfaces [23, 24, 59, 64] and a model of sonoluminescence (an acoustic-induced light emission phenomenon [9, 66]); the latter problem in fact motivates the current study of two-phase flow problems with a van der Waals-type fluid. Our goal here is to establish a basic solution strategy *via* numerical experimentation of some sample problems. Direct simulation of sonoluminescence will be considered in the future.

This paper is organized as follows. In Section 2, we give a full derivation of the model equations that is applicable to two-phase (liquid-gas) flow problems for numerical approximation. In Section 3, we review numerical methods based on wave propagation, and analyze the first-order method for an *interface only* problem. The numerical results are shown in Section 4. This includes a convergence study of the method for a radially symmetric flow and some results on the propagation of shock waves in bubbly liquids. Extension of the method to cases with source terms such as the geometric and gravitational sources is discussed briefly in Section 5. Results of an accuracy study of a spherically symmetric flow is shown also. An overview of the solution procedure to the Riemann problem in a two-phase flow case is demonstrated in Appendix A.

2. Two-Phase (Liquid-Gas) Flow Model. We begin by discussing the basic model equations that are used to describe the motion of the mixture of the liquid and gas components within a grid cell. As a preliminary, a hybrid version of the equation of state is introduced for the liquid-gas mixing cells.

2.1. Equations of state for liquid-gas mixtures. It is known in thermodynamics that an adiabatic version of the van der Waals equation of state (1.2) can be expressed by the form

$$p(\rho) = \mathcal{A}\left(\frac{\rho}{1-\beta\rho}\right)^{\gamma}, \tag{2.1}$$

where as in (1.3) $\mathcal{A}$ is a material constant that is independent of the specific entropy of the gas [21]. From (2.1), the strong resemblance of the equation of state of an adiabatic gas to that of a liquid (1.3) is easily seen. Motivated by this observation, we define a hybrid formulation of (1.3) and (2.1) as follows:

$$p(\rho) = \mathcal{A}\left(\frac{\rho}{1-\beta\rho}\right)^{\gamma} - \mathcal{B}, \tag{2.2}$$

so as to model the basic behavior of a liquid-gas mixture in an adiabatic environment. Clearly, (2.2) reduces to the liquid case (1.3) when $\beta = 0$, and to the gas case (2.1) when $\mathcal{B} = 0$.

But since the problem we are interested in involves the mixing of a non-adiabatic gas and an adiabatic liquid, see Section 1, extension of (2.2) to a general non-adiabatic form needs further considerations. Here we propose an approach by first formulating the internal energy ε in relation to the density ρ alone. This can be done by employing the second law of thermodynamics (cf. [21]) in conjunction with the adiabatic gas assumption and (2.2), yielding to

$$\varepsilon(\rho) = \left(\frac{1-\beta\rho}{\gamma-1}\right)\left(\frac{p(\rho)+\mathcal{B}}{\rho}\right) + \frac{\mathcal{B}}{\rho}. \tag{2.3}$$

By relaxing the solely density-dependence of the internal energy $\varepsilon(\rho)$ to be a more general one such as $\varepsilon(\rho, p)$, we are then able to bring in a new non-adiabatic interpretation of (2.3), and write

$$\varepsilon(\rho, p) = \left(\frac{1-\beta\rho}{\gamma-1}\right)\left(\frac{p+\mathcal{B}}{\rho}\right) + \frac{\mathcal{B}}{\rho}. \tag{2.4}$$

Note that with the use of this so to be called modified van der Waals equation of state (2.4), we recover not only the case (1.2) when $\mathcal{B} = 0$, but also the non-adiabatic version of the case (1.3) (or called the stiffened gas equation of state [52, 53], this is acceptable so along as the entropy change of the liquid is negligible) when $\beta = 0$. If neither β nor $\mathcal{B}$ is equal to zero, (2.4) does give a way to the representation of the cases in between, that is to the mixing of a liquid and gas components. As we will see in the following discussions (cf. [53] also for a simplier case), it is very robust to consider (2.4) as a fundamental element toward the development of a shock-capturing type liquid-gas solver.

For convenience and also for the latter reference, we rewrite (2.4) into a more general class of equation of state as

$$p(\rho, \varepsilon) = \Gamma(\rho)\rho\varepsilon - [\Gamma(\rho) + 1]\,\mathcal{B}. \tag{2.5}$$

Here $\Gamma(\rho)$ denotes the Grüneisen coefficient and is, by assumption, defined to be a positive real value ($\Gamma \in \mathbb{R}_+$) of the form

$$\Gamma(\rho) = \left(\frac{1}{\rho}\right)(\partial_\varepsilon p)\,|_\rho = \frac{\gamma-1}{1-\beta\rho}. \tag{2.6}$$

Note in the other situation, when $\Gamma = (\gamma - 1)/\rho^\alpha$, $\alpha \in (0,1)$ (cf. [41]), for example, (2.5) may be used to model the thermodynamic behavior of the mixing of a solid (condensed matter) and a liquid components. Extension of the work in this direction and in particular to a solid-liquid-gas three-phase flow is in progress, and will be reported elsewhere.

It is worth while mentioning that, with (2.5), the speed of sound c computed by,

$$c^2 = (\partial_\rho p)\,|_{\mathcal{S}} = (\partial_\rho p)\,|_\varepsilon + \left(\frac{p}{\rho^2}\right)(\partial_\varepsilon p)\,|_\rho = \left(\frac{\gamma}{1-\beta\rho}\right)\left(\frac{p+\mathcal{B}}{\rho}\right), \tag{2.7}$$

belongs to a set of positive real numbers ($c \in \mathbb{R}_+$) for all p and ρ in the physical spaces, and γ, β and $\mathcal{B}$ in the parameter spaces, where $\mathcal{S}$ means the specific entropy. Hence there is no phase transition occurring in this two-phase flow model.

2.2. Model equations for liquid-gas mixtures. The basic idea of our approach is quite simple. We use the Euler Eqs. (1.1) as a model system that describes the motion of the mixtures of conserved variables: ρ, ρu, ρv, and ρE, in a liquid-gas coexistent grid cell. We compute the pressure p based on the modified van der Waals equation of state (2.5),

$$p = \left(\frac{\gamma-1}{1-\beta\rho}\right)\left[\rho E - \frac{(\rho u)^2 + (\rho v)^2}{2\rho} - \mathcal{B}\right] - \mathcal{B}, \tag{2.8}$$

so long as the mixture of the problem-dependent material parameters γ, β, and $\mathcal{B}$ are defined and known a priori as well. In the algorithm, by following a general procedure proposed in [52], conditions for those material parameters are found so as to have a consistent approximation of both the internal energy ε and the density ρ on the continuous level. It is important to note that the construction is made with emphasis on (1) the preservation of the pressure in equilibrium for an *interface only* liquid-gas mixture cell, and (2) the conservation of the mixture of the mass on the entire domain. For concreteness, we give a full description of the technique in two space dimensions as follows; the extension of the results to either a higher or lower dimension is straightforward.

Our starting point is to consider an *interface only* problem that the pressure p and the velocity field (u, v) are kept as constants in a two-dimensional domain, while the other variables such as the density ρ and the equation of state parameters: γ, β, and $\mathcal{B}$, are having jumps across a liquid-gas interface. We write Eqs. (1.1) in the following non-conservative form,

$$\begin{aligned}
\partial_t \rho + u\,\partial_x \rho + v\,\partial_y \rho + \rho\,\left(\partial_x u + \partial_y v\right) &= 0, \\
\partial_t u + u\,\partial_x u + v\,\partial_y u + \frac{1}{\rho}\,\partial_x p &= 0, \\
\partial_t v + u\,\partial_x v + v\,\partial_y v + \frac{1}{\rho}\,\partial_y p &= 0, \\
\partial_t(\rho\varepsilon) + \partial_x(\rho\varepsilon u) + \partial_y(\rho\varepsilon v) + p\,\left(\partial_x u + \partial_y v\right) &= 0,
\end{aligned}$$

and obtain easily equations describing the motion of the liquid-gas interface as

$$\partial_t \rho + u\,\partial_x \rho + v\,\partial_y \rho = 0, \tag{2.9a}$$
$$\partial_t(\rho\varepsilon) + u\,\partial_x(\rho\varepsilon) + v\,\partial_y(\rho\varepsilon) = 0. \tag{2.9b}$$

To see how the pressure p would remain in equilibrium as it should be for this model problem, we insert the equation of state (2.5) into (2.9b), and have

$$\partial_t \left[\frac{p+\mathcal{B}}{\Gamma(\rho)} + \mathcal{B}\right] + u\,\partial_x \left[\frac{p+\mathcal{B}}{\Gamma(\rho)} + \mathcal{B}\right] + v\,\partial_y \left[\frac{p+\mathcal{B}}{\Gamma(\rho)} + \mathcal{B}\right] = 0. \tag{2.10}$$

By expanding (2.10), we may therefore write that equation by

$$\left(\frac{1}{\Gamma(\rho)}\right)(\partial_t p + u\,\partial_x p + v\,\partial_y p) + p\,\left(\partial_t \left[\frac{1}{\Gamma(\rho)}\right] + u\,\partial_x \left[\frac{1}{\Gamma(\rho)}\right] + v\,\partial_y \left[\frac{1}{\Gamma(\rho)}\right]\right) + \left(\partial_t \left[\frac{\mathcal{B}}{\Gamma(\rho)} + \mathcal{B}\right] + u\,\partial_x \left[\frac{\mathcal{B}}{\Gamma(\rho)} + \mathcal{B}\right] + v\,\partial_y \left[\frac{\mathcal{B}}{\Gamma(\rho)} + \mathcal{B}\right]\right) = 0,$$

which, on account of the pressure p in equilibrium, comes to a simplier expression

$$p\,\left(\partial_t \left[\frac{1}{\Gamma(\rho)}\right] + u\,\partial_x \left[\frac{1}{\Gamma(\rho)}\right] + v\,\partial_y \left[\frac{1}{\Gamma(\rho)}\right]\right) + \left(\partial_t \left[\frac{\mathcal{B}}{\Gamma(\rho)} + \mathcal{B}\right] + u\,\partial_x \left[\frac{\mathcal{B}}{\Gamma(\rho)} + \mathcal{B}\right] + v\,\partial_y \left[\frac{\mathcal{B}}{\Gamma(\rho)} + \mathcal{B}\right]\right) = 0.$$

Now since this equation should hold for any p in the physical space, it implies right away that the following two terms in the above equation should be vanished simultaneously,

$$\partial_t \left[\frac{1}{\Gamma(\rho)}\right] + u\,\partial_x \left[\frac{1}{\Gamma(\rho)}\right] + v\,\partial_y \left[\frac{1}{\Gamma(\rho)}\right] = 0, \tag{2.11a}$$

$$\partial_t \left[\frac{\mathcal{B}}{\Gamma(\rho)} + \mathcal{B}\right] + u\,\partial_x \left[\frac{\mathcal{B}}{\Gamma(\rho)} + \mathcal{B}\right] + v\,\partial_y \left[\frac{\mathcal{B}}{\Gamma(\rho)} + \mathcal{B}\right] = 0. \tag{2.11b}$$

Notice that (2.11a) and (2.11b) are the two basic evolution equations that should be satisfied for any given expression of the mixture of Γ and $\mathcal{B}$ in order to have the correct pressure behavior in (2.10) for the interface. With the Grüneisen coefficient Γ defined by (2.6), in particular, we find the equations of the form

$$\partial_t \left(\frac{1-\beta\rho}{\gamma-1}\right) + u\,\partial_x \left(\frac{1-\beta\rho}{\gamma-1}\right) + v\,\partial_y \left(\frac{1-\beta\rho}{\gamma-1}\right) = 0, \tag{2.11c}$$

$$\partial_t \left(\frac{\gamma-\beta\rho}{\gamma-1}\mathcal{B}\right) + u\,\partial_x \left(\frac{\gamma-\beta\rho}{\gamma-1}\mathcal{B}\right) + v\,\partial_y \left(\frac{\gamma-\beta\rho}{\gamma-1}\mathcal{B}\right) = 0. \tag{2.11d}$$

From this, we should go further and derive explicit conditions for each of the material parameters γ, β, and $\mathcal{B}$, individually.

It is easy to see that, in addition to (2.11c) and (2.11d), we need to impose one supplementary condition so as to have enough equations for the unknowns. In our approach, this is done by simply splitting (2.11c) into two parts,

$$\partial_t \left(\frac{1}{\gamma-1}\right) + u\,\partial_x \left(\frac{1}{\gamma-1}\right) + v\,\partial_y \left(\frac{1}{\gamma-1}\right) = 0, \tag{2.11e}$$

$$\partial_t \left(\frac{\beta\rho}{\gamma-1}\right) + u\,\partial_x \left(\frac{\beta\rho}{\gamma-1}\right) + v\,\partial_y \left(\frac{\beta\rho}{\gamma-1}\right) = 0. \tag{2.11f}$$

When combining the above equations with (2.11d), we obtain a system of three equations, and that is sufficient to have all the material parameters γ, β, and $\mathcal{B}$ determined at all times. Of course, this is so in case the initial condition has been properly set for the computation, see Section 2.2.1. Note that with ρ and γ computed by (2.9a) and (2.11e), respectively, β can be recovered from (2.11e), and hence $\mathcal{B}$ from (2.11d).

Up to this point, our discussion stresses only on an approach that is capable of maintaining the pressure in equilibrium for a model *interface only* problem. But since in general we are interested in shock wave problems as well, we should thus take the equations, *i.e.*, (2.11d)–(2.11f), in a form that γ, β, and $\mathcal{B}$ remain unchanged across both shocks and rarefaction waves. Because of the involvement of ρ in both (2.11d) and (2.11f), it turns out that for consistency these two equations should be modified in such a way that each of them reduces to the conservation equation of the mass-mixture, when these scenario occur, *i.e.*,

$$\partial_t \left(\frac{\gamma - \beta\rho}{\gamma - 1}\, \mathcal{B} \right) + \partial_x \left(\frac{\gamma - \beta\rho}{\gamma - 1}\, \mathcal{B}u \right) + \partial_y \left(\frac{\gamma - \beta\rho}{\gamma - 1}\, \mathcal{B}v \right) = \left(\frac{\gamma}{\gamma - 1} \mathcal{B} \right) \left(\partial_x u + \partial_y v \right), \tag{2.12a}$$

$$\partial_t \left(\frac{\beta\rho}{\gamma - 1} \right) + \partial_x \left(\frac{\beta\rho}{\gamma - 1} u \right) + \partial_y \left(\frac{\beta\rho}{\gamma - 1} v \right) = 0, \tag{2.12b}$$

for consistency.

To sum up, the model equations we have discussed thus far for a liquid-gas mixture within a grid cell are

$$\left\{ \begin{aligned} & \partial_t \rho + \partial_x (\rho u) + \partial_y (\rho v) = 0 \\ & \partial_t (\rho u) + \partial_x (\rho u^2 + p) + \partial_y (\rho u v) = 0 \\ & \partial_t (\rho v) + \partial_x (\rho u v) + \partial_y (\rho v^2 + p) = 0 \\ & \partial_t (\rho E) + \partial_x (\rho E u + p u) + \partial_y (\rho E v + p v) = 0 \\ & \partial_t \left(\frac{\beta\rho}{\gamma - 1} \right) + \partial_x \left(\frac{\beta\rho}{\gamma - 1} u \right) + \partial_y \left(\frac{\beta\rho}{\gamma - 1} v \right) = 0 \\ & \partial_t \left(\frac{\gamma - \beta\rho}{\gamma - 1}\, \mathcal{B} \right) + \partial_x \left(\frac{\gamma - \beta\rho}{\gamma - 1}\, \mathcal{B}u \right) + \partial_y \left(\frac{\gamma - \beta\rho}{\gamma - 1}\, \mathcal{B}v \right) = \\ & \qquad\qquad\qquad\qquad\qquad \left(\frac{\gamma}{\gamma - 1} \mathcal{B} \right) \left(\partial_x u + \partial_y v \right) \\ & \partial_t \left(\frac{1}{\gamma - 1} \right) + u\, \partial_x \left(\frac{1}{\gamma - 1} \right) + v\, \partial_y \left(\frac{1}{\gamma - 1} \right) = 0. \end{aligned} \right. \tag{2.13}$$

Here in the system the first four equations are simply the Euler Eqs. (1.1) that are used to make certain the conservation of the mixtures ρ, ρu, ρv, and ρE, while the last three equations are (2.11e),(2.12a), and (2.12b), respectively, that are introduced to ensure the correct fluid-mixing of the problem-dependent material variables γ, β, and $\mathcal{B}$ on the interfaces. With a system expressed in this way, there is no problem to compute p from the equation of state (2.8). More detailed discussion of this model will be given in Section 2.3.

2.2.1. Initialization of liquid-gas mixed cells. To begin, let us suppose that for each grid cell we have a volume-fraction function $\mathcal{Z}$ representing the type of fluid within the cell. For instance, for the *liquid-phase only* grid cells we take $\mathcal{Z} = 1$, and therefore for the *gas-phase only* grid cells we assign $\mathcal{Z} = 0$. In case there are some cells cut by the interfaces with $\mathcal{Z} \in (0, 1)$, we then have both the liquid and gas in a cell with which occupied by the volume fractions $\mathcal{Z}$ and $1-\mathcal{Z}$, respectively, see Fig. 1.1 again for a sample grid structure.

Now suppose that for each part of the domain (liquid or gas), the state variables such as $\rho^{(i)}$, $u^{(i)}$, $v^{(i)}$, $p^{(i)}$, $\gamma^{(i)}$, $\beta^{(i)}$, $\mathcal{A}^{(i)}$, and $\mathcal{B}^{(i)}$ are known in advance, for $i = l$ (for liquid) and g (for gas). Note with the equations of state (1.2) and (1.3), for consistency, we should put $\mathcal{A}^{(g)} = \mathcal{B}^{(g)} = \beta^{(l)} = 0$. In this setup, we want to give a proper definition of the fluid mixtures in cells when $\mathcal{Z} \in (0,1)$ that would serves for the initial condition of our model equations (2.13) to the computations.

In the algorithm, we follow a common practice by evaluating the mixing states: ρ, ρu, ρv, and $\rho\varepsilon$, as a volume-weighted sum over the set of the liquid and gas components given above, and find

$$\begin{bmatrix} \rho \\ \rho u \\ \rho v \\ \rho\varepsilon \end{bmatrix} = \mathcal{Z} \begin{bmatrix} \rho^{(l)} \\ \rho^{(l)} u^{(l)} \\ \rho^{(l)} v^{(l)} \\ \rho^{(l)} \varepsilon^{(l)} \end{bmatrix} + (1-\mathcal{Z}) \begin{bmatrix} \rho^{(g)} \\ \rho^{(g)} u^{(g)} \\ \rho^{(g)} v^{(g)} \\ \rho^{(g)} \varepsilon^{(g)} \end{bmatrix}. \tag{2.14}$$

With this result, we then compute the mixture of the total energy by $\rho E = \rho\varepsilon + [(\rho u)^2 + (\rho v)^2]/(2\rho)$; this completes the definition of the conservative variables for the first four equations of (2.13).

To find the fluid mixtures: $1/(\gamma-1)$, $\beta\rho/(\gamma-1)$, and $(\gamma-\beta\rho)\mathcal{B}/(\gamma-1)$, for the remaining part of our model equations (2.13), we use the modified van der Waals equation of state (2.4), where written as a function of the volume fraction it reads

$$\begin{aligned} \left(\frac{1-\beta\rho}{\gamma-1}\right)(p+\mathcal{B}) + \mathcal{B} &= \rho\varepsilon = \mathcal{Z}\rho^{(l)}\varepsilon^{(l)} + (1-\mathcal{Z})\rho^{(g)}\varepsilon^{(g)} \\ &= \mathcal{Z}\left[\left(\frac{p^{(l)}+\mathcal{B}^{(l)}}{\gamma^{(l)}-1}\right) + \mathcal{B}^{(l)}\right] + (1-\mathcal{Z})\left[\left(\frac{1-\beta^{(g)}\rho^{(g)}}{\gamma^{(g)}-1}\right)p^{(g)}\right]. \end{aligned}$$

By taking a similar approach as introduced in Section 2.2 to the derivation of (2.11d)–(2.11f) (cf. [52] also), it comes out readily a splitting of the above equation in the form

$$\begin{bmatrix} \frac{1}{\gamma-1} \\ \frac{\beta\rho}{\gamma-1} \\ \left(\frac{\gamma-\beta\rho}{\gamma-1}\right)\mathcal{B} \end{bmatrix} = \mathcal{Z} \begin{bmatrix} \frac{1}{\gamma^{(l)}-1} \\ 0 \\ \left(\frac{\gamma^{(l)}}{\gamma^{(l)}-1}\right)\mathcal{B}^{(l)} \end{bmatrix} + (1-\mathcal{Z}) \begin{bmatrix} \frac{1}{\gamma^{(g)}-1} \\ \frac{\beta^{(g)}\rho^{(g)}}{\gamma^{(g)}-1} \\ 0 \end{bmatrix} \tag{2.15}$$

with the pressure p governed by the relation

$$\left(\frac{1-\beta\rho}{\gamma-1}\right) p = \mathcal{Z}\left[\frac{p^{(l)}}{\gamma^{(l)}-1}\right] + (1-\mathcal{Z})\left[\left(\frac{1-\beta^{(g)}\rho^{(g)}}{\gamma^{(g)}-1}\right)p^{(g)}\right]. \tag{2.16}$$

With (2.15), it is easy to see that when each of the partial pressures is in equilibrium, the pressure p acquired from (2.16) would remain in equilibrium also, *i.e.*, $p = p^{(l)} = p^{(g)}$. Furthermore, from (2.15), we are able to obtain an explicit expression of the material-dependent parameters γ, β, and $\mathcal{B}$ in terms of both $\mathcal{Z}$ and the original set of data. The results are

$$\gamma = 1 + 1 \Big/ \left[\frac{\mathcal{Z}}{\gamma^{(l)}-1} + \frac{1-\mathcal{Z}}{\gamma^{(g)}-1}\right], \tag{2.17a}$$

$$\beta = (1-\mathcal{Z})\left[\frac{\beta^{(g)}\rho^{(g)}}{\gamma^{(g)}-1}\right] \Big/ \left[\left(\mathcal{Z}\rho^{(l)} + (1-\mathcal{Z})\rho^{(g)}\right)\left(\frac{\mathcal{Z}}{\gamma^{(l)}-1} + \frac{1-\mathcal{Z}}{\gamma^{(g)}-1}\right)\right], \tag{2.17b}$$

$$\mathcal{B} = \left[\frac{\mathcal{Z}\gamma^{(l)}\mathcal{B}^{(l)}}{\gamma^{(l)}-1}\right] \Big/ \left[1 + \frac{\mathcal{Z}}{\gamma^{(l)}-1} + (1-\mathcal{Z})\left(\frac{1-\beta^{(g)}\rho^{(g)}}{\gamma^{(g)}-1}\right)\right]. \tag{2.17c}$$

We note that in case $\mathcal{Z}$ represents a mass-fraction function with $\rho^{(l)} = \rho\mathcal{Z}$ and $\rho^{(g)} = \rho(1-\mathcal{Z})$, relevant mixture states can be defined analogously as in [52].

2.3. A complete model system with volume-fraction function. Before presenting the full set of equations for our two-phase flow application considered here, we describe a simple way to the modeling of the propagation of a liquid-gas interface. We note that this is a necessary step in the algorithm, for we need to know the approximate location of the interface so that suitable system of equations can be applied to each (liquid or gas) part of the domain from the current time to the next.

Similar to the work done in [53], we use the volume-fraction function $\mathcal{Z}$ (see Section 2.2.1) as a key parameter, and have an evolution equation of the form

$$\partial_t \mathcal{Z} + u\,\partial_x \mathcal{Z} + v\,\partial_y \mathcal{Z} = 0 \tag{2.18}$$

to govern the time-dependent behavior of the interface, where (u, v) is the velocity field of the underlying flow. Note that the use of $\mathcal{Z}$ and (2.18) is a popular way in many of the volume-of-fluid type interface tracking methods for interface identification and the subsequent reconstruction (cf. [43, 45, 47, 68]). Clearly, with $\mathcal{Z}$ described by this way, we may use the liquid-phase part of the equations (1.4) and (1.3) when $\mathcal{Z} = 1$, and the gas-phase (including the liquid-gas mixtures) part of the equations (2.13) and (2.4) instead elsewhere. Note that in the latter case, with the coupling of (2.18) to the model, we may simplify the system by removing the transport equation for $1/(\gamma-1)$ from (2.13), and compute γ by (2.17a) (cf. [52, 53]).

In summary, the model equations we propose to solve two-phase (liquid-gas) flow problems consist of the following equations,

$$\left\{\begin{array}{ll}
\partial_t \rho + \partial_x(\rho u) + \partial_y(\rho v) = 0 & \\
\partial_t(\rho u) + \partial_x(\rho u^2 + p) + \partial_y(\rho u v) = 0 & \\
\partial_t(\rho v) + \partial_x(\rho u v) + \partial_y(\rho v^2 + p) = 0 & \\
\partial_t(\rho E) + \partial_x(\rho E u + p u) + \partial_y(\rho E v + p v) = 0 & \text{if} \quad \mathcal{Z} \neq 1 \\
\partial_t\left(\dfrac{\beta\rho}{\gamma-1}\right) + \partial_x\left(\dfrac{\beta\rho}{\gamma-1}u\right) + \partial_y\left(\dfrac{\beta\rho}{\gamma-1}v\right) = 0 & \text{if} \quad \mathcal{Z} \neq 1 \\
\partial_t\left(\dfrac{\gamma-\beta\rho}{\gamma-1}\,\mathcal{B}\right) + \partial_x\left(\dfrac{\gamma-\beta\rho}{\gamma-1}\,\mathcal{B}u\right) + \partial_y\left(\dfrac{\gamma-\beta\rho}{\gamma-1}\,\mathcal{B}v\right) = & \\
\qquad\qquad\qquad \left(\dfrac{\gamma}{\gamma-1}\mathcal{B}\right)(\partial_x u + \partial_y v) & \text{if} \quad \mathcal{Z} \neq 1 \\
\partial_t \mathcal{Z} + u\,\partial_x \mathcal{Z} + v\,\partial_y \mathcal{Z} = 0, &
\end{array}\right. \tag{2.19}$$

where in case $\mathcal{Z} = 1$ the Tait equation of state (1.3) is used to compute p for a liquid, while Eq. (2.8) is employed in the other way.

We note that as in [52, 53] the combined system (2.19) is not written in the full conservation form, but is rather a quasi-conservative system of equations. In addition, the nonzero term on the right-hand side of the second to the last equation should be treated as a part of (2.19), but not be considered as a source term to the system. This fact can be realized readily by formulating (2.19) as a quasi-linear system of equations (of course, with the assumption of a proper smoothness of the solutions), namely,

$$\partial_t q + A(q)\,\partial_x q + B(q)\,\partial_y q = 0 \tag{2.20a}$$

with the state vector

$$q = \left[\rho,\ \rho u,\ \rho v,\ \rho E,\ \frac{\beta\rho}{\gamma-1},\ \frac{\gamma-\beta\rho}{\gamma-1}\mathcal{B},\ \mathcal{Z}\right]^T \tag{2.20b}$$

and the matrices

$$A(q) = \begin{bmatrix} 0 & 1 & 0 & 0 & 0 & 0 & 0 \\ K-u^2 & u(2-\Gamma) & -v\Gamma & \Gamma & p\Gamma & -\Gamma & -p\chi\Gamma \\ -uv & v & u & 0 & 0 & 0 & 0 \\ u(K-H) & H-u^2\Gamma & -uv\Gamma & u(\Gamma+1) & up\Gamma & -u\Gamma & -up\chi\Gamma \\ -\varphi u & \varphi & 0 & 0 & u & 0 & 0 \\ \varphi u\mathcal{B} & -\varphi\mathcal{B} & 0 & 0 & 0 & u & 0 \\ 0 & 0 & 0 & 0 & 0 & 0 & u \end{bmatrix} \tag{2.20c}$$

and

$$B(q) = \begin{bmatrix} 0 & 0 & 1 & 0 & 0 & 0 & 0 \\ -uv & v & u & 0 & 0 & 0 & 0 \\ K-v^2 & -u\Gamma & v(2-\Gamma) & \Gamma & p\Gamma & -\Gamma & -p\chi\Gamma \\ v(K-H) & -uv\Gamma & H-v^2\Gamma & v(\Gamma+1) & vp\Gamma & -v\Gamma & -vp\chi\Gamma \\ -\varphi v & \varphi & 0 & 0 & v & 0 & 0 \\ \varphi v\mathcal{B} & -\varphi\mathcal{B} & 0 & 0 & 0 & v & 0 \\ 0 & 0 & 0 & 0 & 0 & 0 & v \end{bmatrix}. \tag{2.20d}$$

Here $K = \Gamma(u^2+v^2)/2$, $H = E+(p/\rho)$, $\varphi = \beta/(\gamma-1)$, and $\chi = \frac{1}{\gamma^{(l)}-1} - \frac{1}{\gamma^{(g)}-1}$. Recall that Γ is the Grüneisen coefficient, see (2.6), that gives different value for different fluid.

With (2.20a), it is easy to show that Eq. (2.19) is hyperbolic in the sense that any linear combination of the matrices A and B defined above is assumed to have real eigenvalues and a complete set of eigenvectors for each physically relevant values of the state variables q. Regarding discontinuous solutions of the system, such as shock waves or contact discontinuities, Eq. (2.19) has the usual form of the Rankine-Hugoniot jump conditions across the waves, see Appendix A.

To end this section, we write Eq. (2.19) to a more compact expression by

$$\partial_t q + f^{(\partial_x)}(q) + g^{(\partial_y)}(q) = 0, \tag{2.21}$$

where

$$f^{(\partial_x)} = \begin{bmatrix} \partial_x(\rho u) \\ \partial_x(\rho u^2+p) \\ \partial_x(\rho uv) \\ \partial_x(\rho Eu+pu) \\ \partial_x\left(\frac{\beta\rho}{\gamma-1}u\right) \\ u\partial_x\left(\frac{\gamma}{\gamma-1}\mathcal{B}\right) - \partial_x\left(\frac{\beta\rho}{\gamma-1}\mathcal{B}u\right) \\ u\partial_x\mathcal{Z} \end{bmatrix}, g^{(\partial_y)} = \begin{bmatrix} \partial_y(\rho v) \\ \partial_y(\rho uv) \\ \partial_y(\rho v^2+p) \\ \partial_y(\rho Ev+pv) \\ \partial_y\left(\frac{\beta\rho}{\gamma-1}v\right) \\ v\partial_y\left(\frac{\gamma}{\gamma-1}\mathcal{B}\right) - \partial_y\left(\frac{\beta\rho}{\gamma-1}\mathcal{B}v\right) \\ v\partial_y\mathcal{Z} \end{bmatrix}.$$

We note that Eq. (2.21) is written with an understanding that only the first three equations are applicable to the liquid-phase part of the domain when $\mathcal{Z}=1$, but not the remainings.

3. Numerical Methods Based on Wave Propagation. We use the high resolution method based on a wave-propagation viewpoint to compute approximate solutions of our two-phase flow model (2.21) introduced in Section 2.3. The method is a Godunov-type scheme in that we solve the Riemann problems in directions normal and tangential to each cell interface, and propagate the resulting waves (*i.e.*, discontinuities moving at constant speeds) to update the solutions in neighboring grid cells. Similar to many state-of-the-art shock capturing methods, high resolution version of the method can be achieved with the inclusion of slopes and limiters (cf. [22, 28, 29, 30, 33]).

For simplicity in description, we will only briefly discuss the method on a uniform Cartesian grid with fixed mesh spacing $\Delta x = \Delta y = h$, but leave out a more general discussion of the method to nonuniform and time-varying grids, see [37] for the details. We use a standard finite-volume formulation in which the value Q_{ij}^n approximates the cell average of the solution over the (i,j)th grid cell at time t_n,

$$Q_{ij}^n \approx \frac{1}{h^2} \int_{C_{ij}} q(x,y,t_n)\; dx\; dy,$$

where C_{ij} denotes the region occupied by grid cell (i,j). The time step is denoted by k.

3.1. First order methods. To begin, consider the interface between cells $(i-1,j)$ and (i,j), for example. We solve the one-dimensional Riemann problem normal to this face, which in this case will be

$$\partial_t q + f^{(\partial_x)}(q) = 0, \tag{3.1}$$

with initial data given by $Q_{i-1,j}^n$ and Q_{ij}^n. We use a simplified version of the exact Riemann solver based on the shock-only approximation (cf. [10, 13]), and find the solution consisting of three discontinuities propagating at constant speeds, see Appendix A. The jump across each discontinuity is the difference between the state variables of the form,

$$\mathcal{W}_1 = q_{*L} - Q_{i-1,j}^n, \qquad \mathcal{W}_2 = q_{*R} - q_{*L}, \qquad \text{and} \qquad \mathcal{W}_3 = Q_{ij}^n - q_{*R},$$

and the propagating speed is the corresponding shock speed with the exception of the λ_2 wave family for the contact discontinuity. Here q_{*L} and q_{*R} are the state vectors defined to the left and right of the 2th wave from the Riemann problem solution. Note that with this type of Riemann solver we have the usual splitting of jumps into waves,

$$Q_{ij}^n - Q_{i-1,j}^n = \sum_{m=1}^{3} \mathcal{W}_m.$$

It is widely conceived that numerical methods based on an exact Riemann solver of the kind used here would generally cost too much as compared to that based on an approximate Riemann solver, *e.g.*, the method of Roe [48]. But due to the stiffness of the equations of state for the liquid and gas under studied, we find it is the only accurate way to perform so as to have a proper resolution of the solution near the liquid-gas interfaces. Clearly, to improve efficiency of the solution step in solving the Riemann problems, one may adapt a hybrid formulation that utilizes the approximate Riemann solver exclusively in regions with a single phase of the fluid, but employs the exact solver otherwise (we will not pursued this point further to keep the implementation of the algorithm simple).

Now if the wave speed $\lambda_l < 0$, the lth wave propagates into cell $(i-1, j)$, while if $\lambda_l > 0$ it propagates into cell (i, j). In the simplest case of the wave propagation method, *i.e.*, a two-dimensional extension of Godunov's method, the cell average affected by this wave is simply updated by $(kh\lambda_l/h^2)\mathcal{W}_l$. Note that the quantity in parentheses is the fraction of the cell swept out by this wave, see Fig. 3.1a. By computing the effect of each wave to the cell averages, a single time step of the solution algorithm is completed.

It is well-known that this first order algorithm has a very limited time step restriction for stability [30]. Here by following an approach proposed in [28], we improve upon the algorithm by introducing "transverse propagation" of these waves, so that they affect the cells above or below row j as well, based on the propagation speeds in the y-direction. We do this for each wave individually, where we solve a Riemann problem for the equation

$$\partial_t q + g^{(\partial_y)}(q) = 0 \tag{3.2}$$

and data Q_L and Q_R just to the left and right of the wave. Considering the lth wave mentioned above, for example. This amounts to setting

$$Q_L = Q^n_{i-1,j} + \sum_{m=1}^{l-1} \mathcal{W}_m, \qquad Q_R = Q_L + \mathcal{W}_l,$$

and leads to a splitting of the wave into 3 pieces,

$$\mathcal{W}_l = Q_R - Q_L = \sum_{m=1}^{3} \mathcal{W}_{lm},$$

where each sub-wave propagates at a speed μ_m in the y-direction, for $m = 1, 2, 3$. Fig. 3.1b shows a typical example of the $\mu_m > 0$ case, where the wave $\mathcal{W}_{lm}$ is used to update the cell averages in cells (i, j) and $(i, j+1)$, based on the area that the wave overlaps each cell,

$$\begin{aligned} Q^{n+1}_{ij} &:= Q^{n+1}_{ij} - \left(\frac{k\lambda_l}{h}\right)\left(1 - \frac{1}{2}\frac{k\mu_m}{h}\right)\mathcal{W}_{lm}, \\ Q^{n+1}_{i,j+1} &:= Q^{n+1}_{i,j+1} - \frac{1}{2}\left(\frac{k^2\lambda_l\mu_m}{h^2}\right)\mathcal{W}_{lm}. \end{aligned}$$

Note that we have employed a standard initialization procedure that assigns each cell average to its values at the previous time step,

$$Q^{n+1}_{ij} = Q^n_{ij} \qquad \text{for all } i,\ j.$$

It should be mentioned that there exists an alternative transverse-propagation approach based on the splitting of numerical upwind or downwind fluxes instead (cf. [31, 33, 38]). This latter approach is often useful for a flux formulation of the wave-propagation schemes, whenever the equations to be solved can be written in the full conservation form, such as the single component of the Euler equations of gas dynamics. Here because our model system (2.21) is written in a quasi-conservative

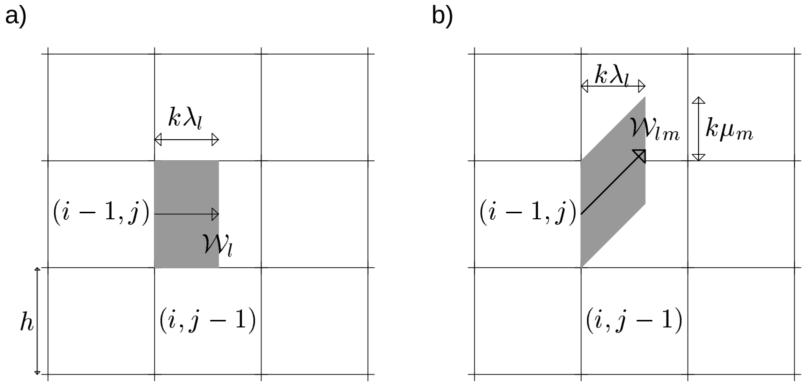

FIG. 3.1. *First order wave propagation method. (a) Normal wave propagation, a case with $\lambda_l > 0$ is shown. (b) Transverse wave propagation, a case with the splitting of the lth wave shown in (a). Only the mth sub-wave is plotted, $\mu_m > 0$. The cell averages affected by the shaded region of the wave is updated.*

form, it is not convenient to use that method as a basis for numerical approximation (cf. [49, 50] for a related work). In fact, we find it is robust to use the method in wave-propagation form that we are able to handle each wave in turn, and there is no need to compute fluxes and make distinction between the waves.

Undoubtedly, this modified version of the Godunov's method belongs to a class of unsplit multidimensional upwind schemes. For a scalar problem, in particular, this approach is a variant of the corner transport upwind method of Colella [11] in that the cell averages at the next time step can be interpreted as a linear combination of the neighboring cell values at the old time with suitable weights. To make this clear (see [32] also), we consider a linear advection equation

$$\partial_t q + u\, \partial_x q + v\, \partial_y q = 0,$$

with a positive velocity field $(u, v) > 0$, $q \in \mathbb{R}$, as an example. Denote $\nu_x = ku/h$ and $\nu_y = kv/h$. The update of the cell average in terms of the jumps across each cell interface, say for the case of Q_{ij}^n shown in Fig. 3.1b for example, can be found by

$$\begin{aligned} Q_{ij}^{n+1} = Q_{ij}^n &- \nu_x \left(1 - \frac{1}{2}\nu_y\right) \left(Q_{ij}^n - Q_{i-1,j}^n\right) - \nu_y \left(1 - \frac{1}{2}\nu_x\right) \left(Q_{ij}^n - Q_{i,j-1}^n\right) \\ &- \frac{1}{2}\nu_x\nu_y \left(Q_{i,j-1}^n - Q_{i-1,j-1}^n\right) - \frac{1}{2}\nu_x\nu_y \left(Q_{i-1,j}^n - Q_{i-1,j-1}^n\right). \end{aligned} \tag{3.3}$$

After a simple reorganization of terms, it can then be viewed as a sum of the transport of the neighboring states into the cell,

$$Q_{ij}^{n+1} = (1 - \nu_x - \nu_y) Q_{ij}^n + \nu_x (1 - \nu_y)\, Q_{i-1,j}^n + \nu_y (1 - \nu_x)\, Q_{i,j-1}^n + \nu_x\nu_y Q_{i-1,j-1}^n,$$

within a time step k (cf. Fig. 1 of [11]). For convenience, we may write the above scheme to a more general form

$$Q_{ij}^{n+1} = \sum_{l=0}^{1} \sum_{m=0}^{1} \alpha_{lm}\, Q_{i-l,j-m}^n, \tag{3.4}$$

with the coefficients defined by $\alpha_{00} = (1-\nu_x-\nu_y)$, $\alpha_{1,0} = \nu_x(1-\nu_y)$, $\alpha_{0,1} = \nu_y(1-\nu_x)$, and $\alpha_{1,1} = \nu_x\nu_y$. The method is clearly a monotone scheme, and hence first-order accurate, as long as the time step k satisfies the CFL condition $\max(\nu_x, \nu_y) \le 1$. Concerning stability of the full nonlinear system (2.21), it is observed numerically that the method is stable and convergent under mesh refinement provided that the waves in the method affect only the cells adjacent to the interface during the time step, see Section 4 for numerical examples and also the results shown in [33].

We next show that in case of an *interface only* problem (see Section 2.2) the pressure p obtained using the method would remain in equilibrium without any spurious oscillations near the gas-liquid interfaces. Without loss of generality, we consider a square gas bubble with mesh-alignment interface occupied the entire (i,j)th grid cell, while outside the gas bubble, the fluid contains liquids wholely. We pick up the initial data so that there are no jumps in both the pressure p and velocities (u,v), but is otherwise for the other variables such as ρ, γ, β, and $\mathcal{B}$ across the bubble interface. Assuming a positive velocity field $(u,v) > 0$, the solution of (2.21) by the "transverse-propagation" version of the method for the problem can be shown to satisfy a vector form of (3.4) with Q_{ij}^n representing the numerical approximation of the vector q defined in (2.20b), *i.e.*,

$$Q_{ij}^{n+1} = \begin{bmatrix} \rho \\ \rho u \\ \rho v \\ \rho E \\ \frac{\beta\rho}{\gamma-1} \\ \frac{\gamma-\beta\rho}{\gamma-1}\mathcal{B} \\ \mathcal{Z} \end{bmatrix}_{ij}^{n+1} = \sum_{l=0}^{1}\sum_{m=0}^{1} \alpha_{lm} \begin{bmatrix} \rho \\ \rho u \\ \rho v \\ \rho E \\ \frac{\beta\rho}{\gamma-1} \\ \frac{\gamma-\beta\rho}{\gamma-1}\mathcal{B} \\ \mathcal{Z} \end{bmatrix}_{i-l,j-m}^{n}. \tag{3.5}$$

From the first three components of Eq. (3.5), it is an easy matter to check the fulfillment of the uniform velocity condition: $(u,v)_{ij}^{n+1} = (u,v)_{ij}^n$, for all i, j. Having known this, the fourth component of Eq. (3.5) can be simplified to

$$(\rho\varepsilon)_{ij}^{n+1} = \sum_{l=0}^{1}\sum_{m=0}^{1} \alpha_{lm}\ (\rho\varepsilon)_{i-l,j-m}^{n}.$$

When substituting the modified van der Waals equation of state (2.4) for $\rho\varepsilon$ into the above formula, it gives the definition of the liquid-gas mixture for $\rho\varepsilon$,

$$\begin{aligned} \left[\left(\frac{1-\beta\rho}{\gamma-1}\right)(p+\mathcal{B})+\mathcal{B}\right]_{ij}^{n+1} = \alpha_{00}\left[\left(\frac{1-\beta\rho}{\gamma-1}\right)\ p\right]_{ij}^{n} + \alpha_{10}\left(\frac{p+\gamma\mathcal{B}}{\gamma-1}\right)_{i-1,j}^{n} + {} \\ \alpha_{01}\left(\frac{p+\gamma\mathcal{B}}{\gamma-1}\right)_{i,j-1}^{n} + \alpha_{11}\left(\frac{p+\gamma\mathcal{B}}{\gamma-1}\right)_{i-1,j-1}^{n}, \end{aligned} \tag{3.6}$$

where at time t_n (before the mixing of the liquid and gas), we have set $\mathcal{B} = 0$ for a van der Waals gas, see (1.2), and $\beta = 0$ for the liquid, see Section 2.1. Note that the pressure for either the liquid or gas is in the equilibrium state p_0 before the update, *i.e.*, $p_{ij}^n = p_{i-1,j}^n = p_{i,j-1}^n = p_{i-1,j-1}^n = p_0$. By following an approach described in [52] for a multicomponent model in one dimension (see Section 2.2 also for the basic idea), it is not difficult to show the satisfaction of the pressure equilibrium $p_{ij}^{n+1} = p_0$, for all i, j, obtained using the method, so long as $\rho\varepsilon$ is computed by (3.6) and the other variables such as: ρ, β, $\mathcal{B}$, and $\mathcal{Z}$ (and so γ), are set by (3.5).

3.2. High resolution corrections. Here we discuss the high-resolution version of the wave propagation method for numerical approximation of Eq. (2.21). To fix the idea, we begin by looking at the Taylor series expansion of the state vectors $q(x, y, t+k)$ at time t,

$$\begin{aligned} q(x,y,t+k) &= q(x,y,t) + k\,\partial_t q(x,y,t) + \frac{1}{2}k^2\,\partial_{tt} q(x,y,t) + \cdots, \\ &= q(x,y,t) - k\,\left(A\,\partial_x q + B\,\partial_y q\right)(x,y,t) + \frac{1}{2}k^2\,\left[\partial_x(A^2\,\partial_x q) + \right. \\ &\qquad \left. \partial_x(AB\,\partial_y q) + \partial_y(BA\,\partial_x q) + \partial_y(B^2\,\partial_y q)\right](x,y,t) + \cdots, \end{aligned} \tag{3.7}$$

where with the aid of Eq. (2.20a) we have replaced the time derivatives $\partial_t q$ and $\partial_{tt} q$ by the respective spatial derivatives. Clearly, from the basic local truncation error analysis, to achieve second-order accuracy of the method, we need to include an approximation to the term

$$\partial_{tt} q = \partial_x(A^2\,\partial_x q) + \partial_x(AB\,\partial_y q) + \partial_y(BA\,\partial_x q) + \partial_y(B^2\,\partial_y q).$$

In pursuit of implementing this efficiently, it turns out that the transverse-wave splitting method described in Section 3.1 has already given a way to approximate the terms: $\partial_x(AB\,\partial_y q)$ and $\partial_y(BA\,\partial_x q)$, see [31] for the details. Thus, to achieve full second-order accuracy, we need only add in the $\partial_x(A^2\,\partial_x q)$ and $\partial_y(B^2\,\partial_y q)$ terms to the method. As in the one-dimensional case (cf. [36]), one standard procedure to do this is to first introduce correction waves in a piecewise-linear form, propagate the wave normal to the interface over the time step k, and then update the cell averages it overlaps.

Consider the lth wave shown in Fig. 3.2a, for example. The corrections are accomplished by the updates

$$\begin{aligned} Q_{ij}^{n+1} &:= Q_{ij}^{n+1} + \frac{1}{2}\left(\frac{k\lambda_l}{h}\right)\left(1 - \frac{k\lambda_l}{h}\right)\mathcal{W}_l, \\ Q_{i-1,j}^{n+1} &:= Q_{i-1,j}^{n+1} - \frac{1}{2}\left(\frac{k\lambda_l}{h}\right)\left(1 - \frac{k\lambda_l}{h}\right)\mathcal{W}_l, \end{aligned}$$

where the factors multiplying $\mathcal{W}_l$ are simply the fractions of each cell that is overlapped by the correction wave. In practice, the strength of each wave is limited using a "slope-limiter" [58], and so each $\mathcal{W}_l$ in the above correction is replaced by a limited value $\widetilde{\mathcal{W}_l}$ obtained by comparing $\mathcal{W}_l$ with the corresponding $\mathcal{W}_l$ from the neighboring Riemann problem to the left (if $\lambda_l > 0$) or to the right (if $\lambda_l < 0$). Note that the correction wave is constructed in such a way that the total contribution of the wave to cell averages is equal to zero, irrespective with any choice of slopes. More details can be found in [28, 29, 33], but they will not be repeated here.

It should be noted that we may improve upon the method (but is still second-order accurate) by introducing transverse propagation of correction waves as well. In this instance, the $\mathcal{W}_{lm}$ (see Section 3.1) is used to update cell averages whichever it

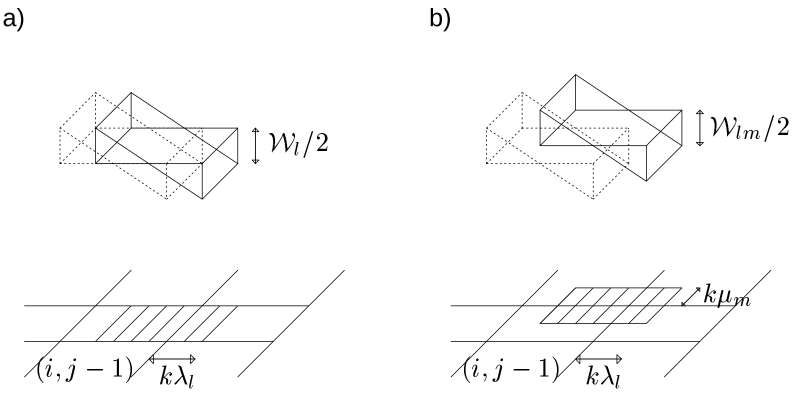

FIG. 3.2. *High-resolution wave propagation methods. (a) Normal propagation of correction wave, a case with $\lambda_l > 0$ is shown. (b) Transverse propagation of correction wave, a case with the splitting of the lth wave shown in (a). Only the mth sub-wave is plotted, $\mu_m > 0$. The piecewise-linear wave form in dashed lines is the initial location of the correction wave before propagation. The cell averages affected by the correction wave is updated by the volume of the interaction between the wave and grid cell.*

is affected, see Fig. 3.2b. The updates are

$$
\begin{aligned}
Q_{ij}^{n+1} &:= Q_{ij}^{n+1} + \frac{1}{2}\left(\frac{k\lambda_l}{h}\right)\left(1-\frac{k\lambda_l}{h}\right)\left(1-\frac{k\mu_m}{h}\right)\mathcal{W}_{lm}, \\
Q_{i-1,j}^{n+1} &:= Q_{i-1,j}^{n+1} - \frac{1}{2}\left(\frac{k\lambda_l}{h}\right)\left(1-\frac{k\lambda_l}{h}\right)\left(1-\frac{k\mu_m}{h}\right)\mathcal{W}_{lm}, \\
Q_{i,j+1}^{n+1} &:= Q_{i,j+1}^{n+1} + \frac{1}{2}\left(\frac{k\lambda_l}{h}\right)\left(1-\frac{k\lambda_l}{h}\right)\left(\frac{k\mu_m}{h}\right)\mathcal{W}_{lm}, \\
Q_{i-1,j+1}^{n+1} &:= Q_{i-1,j+1}^{n+1} - \frac{1}{2}\left(\frac{k\lambda_l}{h}\right)\left(1-\frac{k\lambda_l}{h}\right)\left(\frac{k\mu_m}{h}\right)\mathcal{W}_{lm}.
\end{aligned}
$$

It can be shown that when handling all the correction waves in this way, we have a consistent approximation to the third order terms: $BA^2\ \partial_{xxy}q$ and $AB^2\ \partial_{yyx}q$, see [32] for a detailed analysis to a scalar problem. Based on various numerical evidences, we find this modified method with transverse propagation of correction waves works slightly better than that with normal propagation of the waves (judging from preserving symmetry of the solutions, for example). Hence, the numerical results present in the paper use exclusively the transverse-propagation version of the high resolution method for experiments. Validation of the method to an *interface only* problem will be carried out *via* numerical computations in the next Section.

4. Numerical Results. We now present results of some sample calculations obtained using our two-phase flow algorithm proposed in the previous sections.

4.1. Evolution of a single bubble. We begin by considering an *interface only* problem that the solution consists of a circular gas bubble evolving in a liquid with uniform equilibrium pressure $p_0 = 1$ and constant velocity field $(u_0, v_0) = (1, 1)$. We use the same setup as done in [52] that, inside a circular region $r \le 0.16$, the fluid is a van der Waals-type gas with the density $\rho^{(g)} = 1$, the adiabatic gas constant $\gamma^{(g)} = 1.4$, and the van der Waals excluded volume constant $\beta^{(g)} = 0.036$, while outside the circular region $r > 0.16$, the fluid is a liquid with $\rho^{(l)}$ determined by

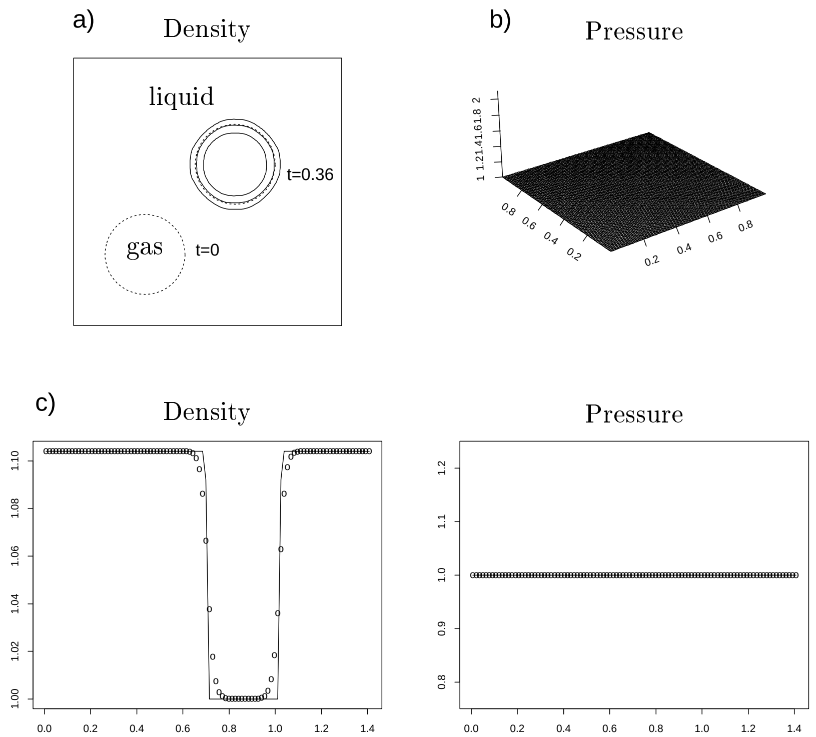

FIG. 4.1. *High-resolution results for an interface-evolving problem at time $t = 0.36$. (a) Contour plot of the density ρ. (b) Surface plot of the pressure p. (c) Cross-sectional plots of ρ and p along line $x = y$. The solid line in the cross-sectional plot is the exact solution, and the dotted points are the numerical results. The dashed lines in the density contour plot are the exact location of the moving bubble at both the initial time $t = 0$, and the final stopping time $t = 0.36$.*

both the uniform pressure p_0 and the Tait equation of state (1.3) of parameter values: $\mathcal{A}^{(l)} = 1$, $\mathcal{B}^{(l)} = 1$, and $\gamma^{(l)} = 7$. Here $r^2 = (x - x_0)^2 + (y - y_0)^2$ is the distance from a point (x, y) in a unit square domain to the center of the bubble $(x_0, y_0) = (\frac{1}{4}, \frac{1}{4})$.

The results of one sample test are shown in Fig. 4.1 where the contours of the density ρ, the surface plot of the pressure p, and the cross section of ρ and p along the $x = y$ line are presented at a selected time $t = 0.36$. From the figure, it is easy to observe good agreement of the numerical solutions as compared with the exact results. Notice in particular that the computed pressure remains in equilibrium as desired, without any spurious oscillations near the bubble interface. In this computation we have used a high-resolution version of the method with a 100×100 grid, a fixed time step $k = 2 \cdot 10^{-3}$ (which amounts to using the Courant number 0.9 approximately), and the "minmod" limiter [30]. Non-reflecting outflow boundary conditions were employed on each outer side of the unit square domain.

4.2. A radially symmetric flow. We next consider problems with geometric symmetry (*eg*, radial symmetry) that the computed solutions in two dimensions can be compared to the one-dimensional results for numerical validation. We use the following set of two-phase (liquid-gas) flow data for experiments in which, in the gas-phase, the state variables are

$$(\rho,\ p,\ \gamma,\ \beta)^{(g)} = (1.25,\ 2.75,\ 1.4,\ 0.036) \qquad \text{for} \quad r \le \frac{1}{5},$$

while, in the liquid-phase, they are

$$(\rho,\ p,\ \gamma,\ \mathcal{A},\ \mathcal{B})^{(l)} = (1,\ 0,\ 7,\ 1,\ 1) \qquad \text{for} \quad r > \frac{1}{5},$$

where $r^2 = x^2 + y^2$. Initially both the gas and liquid are in a stationary position, but due to the pressure difference between the fluids, breaking of the circular membrane at $r = \frac{1}{5}$ occurs instantaneously. For this problem, the resulting solution consists of an outward-going shock wave in liquid, an inward-going rarefaction wave in gas, and a contact discontinuity lying in between that separates the gas and the liquid. We note that because of the symmetry of the solution, for simplicity, we only take a quarter of the unit square domain, *i.e.*, $(x, y) \in ([0, \frac{1}{2}] \times [0, \frac{1}{2}])$, and apply the line of symmetry boundary conditions on both the bottom and the left boundaries for the computation.

In Fig. 4.2, we show numerical results for both ρ and p at time $t = 0.07$, where as in the previous example the test is performed using a 100×100 grid with the high-resolution method. Clearly, the contours shown in Fig. 4.2a give good resolution of the wave pattern after the breaking of the membrane, where the dashed line in the contours of p is the approximate location of the interface. The scatter plots shown in Fig. 4.2b provide the validation of our two-dimensional results as in comparison with the "true" solution obtained from solving the one-dimensional model with appropriate source terms for the radial symmetry (see Section 5), using the high-resolution method with mesh size $h = \frac{1}{2000}$. See [53] for a similar calculation in which a simplier case with $\beta^{(g)} = 0$ was considered in the test.

A more detailed study of the solutions under mesh refinement is presented in Table 4.1 that in the 1-norm the method is convergent at a rate of 0.95 for ρ, 1.01 for $\rho\bar{u}$ (where $\bar{u}^2 = u^2 + v^2$), and 0.81 for ρE. In the max-norm, however, the rate of convergence of the method is significantly lower than the ones to the 1-norm case. It should be noted that the convergence rate shown in Table 4.1 is typical when using the state-of-the-art shock capturing methods for discontinuous solutions (see [36, 37, 54] for some additional examples). That is to say, our two-phase flow algorithm works just as good as standard methods for a single-component problem.

Note in Table 4.1, the number in the parenthesis represents the exponent of the base 10, for example, $2.331(-3)$ means $2.331 \cdot 10^{-3}$. The order of accuracy of a method is computed by performing a standard linear least-squares fit to a sequence of mesh refinement data shown in the table, and take the slope as the order of accuracy of the method (cf. [37]).

4.3. Shock-bubble interaction. We now present results to the simulation of a shock wave in bubbly liquids. The aim of the test performed here is twofold: the first is to validate convergence of the computed solutions obtained using our two-phase flow algorithm to the correct weak ones, and the second is to provide an example that shows the feasibility of the algorithm to practical problems. Note this problem is of practical importance to many applications in sciences and engineering (see [7, 9, 16] and references therein for more information).

To setup the test, we consider a downward-moving Mach 1.587 shock wave in

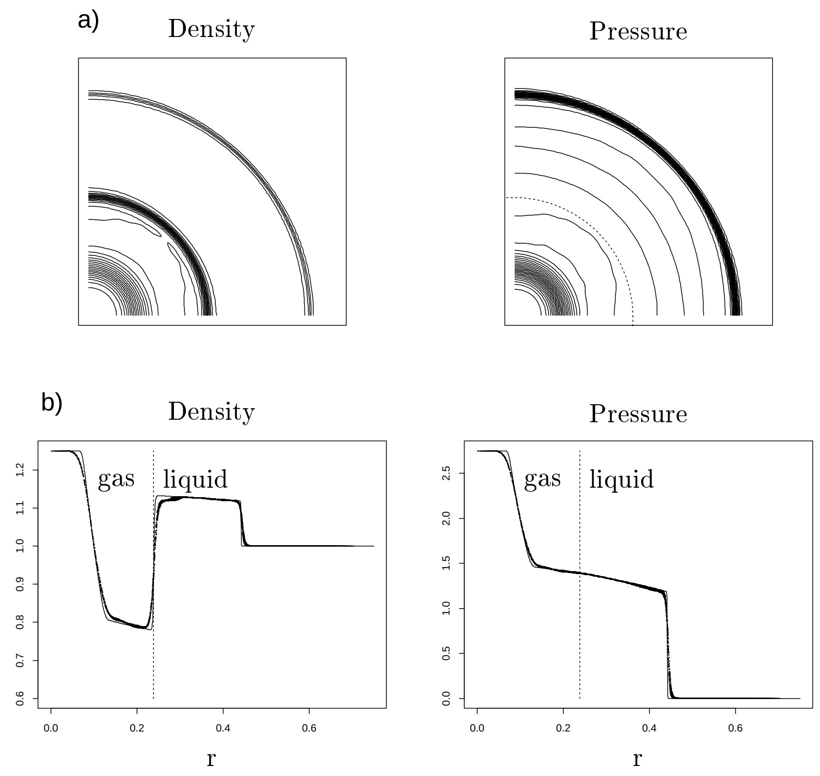

FIG. 4.2. *High-resolution results for a radially symmetric problem at time $t = 0.07$. (a) Contours of the density ρ and the pressure p. (b) Scatter plots of ρ and p with locations measured as a distance from the cell center to the origin. The solid line in the scatter plot is the "true" solution obtained from solving the one-dimensional model with appropriate source terms for the radial symmetry using the high-resolution method. The dotted points are the two-dimensional result. The dashed line shown in the figure is the approximate location of the interface.*

TABLE 4.1
An accuracy study for a radially symmetric problem

	1-norm			max-norm		
N	ρ	$\rho\bar{u}$	ρE	ρ	$\rho\bar{u}$	ρE
50	2.331(−3)	1.870(−3)	7.448(−3)	9.847(−2)	1.905(−1)	4.715(−1)
100	1.246(−3)	9.678(−4)	4.512(−3)	9.363(−2)	1.693(−1)	4.679(−1)
200	6.224(−4)	4.582(−4)	2.413(−4)	8.260(−2)	1.345(−1)	3.867(−1)
order	0.95	1.01	0.81	0.1	0.25	0.14

Note. Global errors are shown with notation defined in the text. The computational grid is $N \times N$.

water with data in the preshock state,

$$(\rho,\ u,\ v,\ p)^{(w)}_{\text{preshock}} = (1,\ 0,\ 0,\ 1),$$

and data in the post-shock state,

$$(\rho,\ u,\ v,\ p)^{(w)}_{\text{post-shock}} = (1.2330,\ 0,\ -43.4665,\ 10^4).$$

The equation of state parameters we employed for the water, *i.e.*, (1.3), are standard, where $\mathcal{A}^{(w)} = 3001$ atm, $\mathcal{B}^{(w)} = 3000$ atm, and $\gamma^{(w)} = 7$ (cf. [15]). In addition to the shock wave, we assume there is a set of stationary air bubbles of finite size located just below the shock in which some of them are about to interact with the shock, see Fig. 4.3 or 4.6 for an illustration. Inside each of the bubbles of air, the state variables are assigned by $\rho^{(a)} = 1.2 \cdot 10^{-3}$ (dimensional unit g/cc), $p^{(a)} = 1$, $\gamma^{(a)} = 1.4$, and $\beta^{(a)} = 3.6 \cdot 10^{-5}$ for a van der Waals gas (1.2) (cf. [66]). We note that because of the large pressure jump across the shock wave and also the large ratio of acoustic impedances of the water to air, $(\rho c)^{(w)}/(\rho c)^{(a)} \approx 3535$, this is a much more severe test than those ones considered previously in this section, and also in [52]; c is the speed of the sound of the material of interests.

4.3.1. Single bubble case. To begin, the experiment is carried out with only a single gas bubble. Figs. 4.3 and 4.4 show high-resolution results of a sample run using a 200×240 grid on a $[0, 1] \times [-0.2, 1]$ rectangular domain (non-reflecting outflow boundary conditions are used on the boundaries). In Fig. 4.3, reasonable resolution of the solution structure (cf. [18, 24, 46] of a similar test) are obtained using the algorithm where contours of ρ, p, and $\mathcal{Z}$ are presented at five different times, $t = (1, 2, 3, 4, 5) \cdot 10^{-3}$, ($\rho$ and p are plotted in logarithmic scale). The cross section of the results for the same run along line $x = \frac{1}{2}$ is presented in Fig. 4.4. Notice, in particular, that the pressure is free of spurious oscillations near the interface, when $\mathcal{Z} \neq 1$.

To check the correctness of the computed solutions, Fig. 4.5 shows results of a convergence study of ρ and p along line $x = \frac{1}{2}$ and at time $t = 5 \cdot 10^{-3}$. Noticing the sensible convergence behavior of the solution profiles under mesh refinement, where we have use a grid sequence: $2^i(50 \times 60)$ for $i = 0, 1, 2$, for the test.

4.3.2. Multiple bubble case. Finally, the propagation of a shock wave over an array of air bubbles is under investigation. We use the same initial condition as done in Section 4.3.1, but with a combination of circular and elliptical air bubbles distributed rather randomly as shown in Fig. 1.1 for the computation. Figs. 4.6–4.8 show numerical results of a similar run as performed in the previous example. Clearly, from the contours of the plot, Fig. 4.6, the distortion of the air bubbles and the somewhat chaotic wave patterns are visible after the passage of the shock wave to bubbles. In Fig. 4.8, we again observe the reasonable convergence behavior of the solutions, when the mesh is refined, and the final stopping time is fixed to $t = 5 \cdot 10^{-3}$. It should be mentioned that the oscillatory wave train of the pressure behind the incident shock wave, see Fig. 4.8, is one of the typical phenomena during the propagation of shocks in bubbly liquids (cf. [44]).

It is interesting to note that, in a future work, we plan to use the proposed method as a tool to study general wave propagation phenomena in bubbly liquids. Comparison of the direct numerical simulation results with those obtained from standard homogenization theory for bubbly liquids [5, 6, 64, 65] and with the related laboratory experiments [44, 59] will be looked at closely.

5. Source Terms. To show how to include source terms to our two-phase flow algorithm, we make a simple generalization of Eq. (2.19) to a spherically-symmetric version of the model in two dimensions, *i.e.*,

$$\partial_t q + f^{(\partial_r)}(q) + g^{(\partial_z)}(q) = \psi(q), \tag{5.1a}$$

TABLE 5.1
An accuracy study for a spherically symmetric problem

	1-norm			max-norm		
N	ρ	$\rho\bar{u}$	ρE	ρ	$\rho\bar{u}$	ρE
50	$2.269(-3)$	$1.566(-3)$	$6.315(-3)$	$1.261(-1)$	$1.237(-1)$	$5.200(-1)$
100	$1.304(-3)$	$9.212(-4)$	$3.669(-3)$	$1.224(-1)$	$1.143(-1)$	$3.678(-1)$
200	$6.813(-4)$	$4.772(-4)$	$1.914(-3)$	$1.067(-1)$	$1.025(-1)$	$2.290(-1)$
order	0.87	0.85	0.86	0.12	0.14	0.59

Note. The notation are defined in the same way as in Table 4.1.

with

$$\psi(q) = -\frac{1}{r}\left[\rho u,\ \rho u^2,\ \rho uv,\ \rho E u + pu,\ \frac{\beta\rho}{\gamma-1}u,\ \frac{\beta\rho}{\gamma-1}\mathcal{B}u,\ 0\right]^T, \tag{5.1b}$$

where u and v denote the velocities in the r- (radial) and z-direction, respectively; $r^2 = x^2+y^2$. Here the source term ψ on the right hand side of Eq. (5.1a) comes directly from the geometric simplification of a three-dimensional flow to a two-dimensional one. Notice that Eq. (5.1a) is taken of the form that reduces to a typical single-phase flow model, when there is no jump on each of the material-dependent constants γ, β, $\mathcal{A}$, and $\mathcal{B}$ across the interfaces.

Results of a spherically-symmetric run that is similar to the case shown in Fig. 4.2 are presented in Fig. 5.1, where the scatter plots of ρ and p are displayed at time $t = 0.07$ using a 100×100 grid (cf. [17]). Convergence of the solution is clearly observed for data given in Table 5.1 where an accuracy study of the method is carried out with three different mesh size: $2^i \cdot (50 \times 50)$, $i = 0, 1, 2$. Again, we have computed the "true" solution of the problem by treating a one-dimensional model with a source term for spherical symmetry. Here numerical approximation based on a Strang-type time splitting procedure [55] is used to handle to source terms of Eq. (5.1a) in a high-resolution manner.

Note if gravity (which acts as a body force to the system) is of importance in the simulation, such as for water-drop or rising-bubble problems, gravitational source terms of the form,

$$\psi(q) = [0,\ 0,\ \rho g_0,\ \rho g_0 v,\ 0,\ 0,\ 0]^T, \tag{5.2}$$

should be included to the model equations, *i.e.*, to either Eq. (2.19) for 2D, or Eq. (5.1a) for 3D problems, where g_0 is the gravitational acceleration constant. Because it requires some special attentions to the treatment of the gravity source (5.2), see [34, 35], we will not present any more numerical results here, but refer to a paper in preparation [51], where an adaptive grid approach will be included to the simulations.

6. Conclusions. We have described and validated a two-phase (liquid-gas) flow algorithm with or without source terms in two space dimensions. The algorithm uses a mixture-type of the governing equations together with a hybrid equation of state for the modeling of fluid mixing between liquids and gases on the macroscopic level. An evolution equation for the volume-fraction of the liquid within a cell is introduced that gives approximate location of the interface from the current time to the next. A complete two-phase flow model written in quasi-conservative form is solved using the standard high-resolution method based on the wave-propagation formulation that is robust for the current application. Validation of the approach is clearly established by numerical results present in the paper.

Ongoing work is to further improve upon efficiency and resolution of the algorithm by combining an adaptive mesh refinement technique (cf. [3, 4]) to the existing computer program. Direct numerical simulation of practical problems, such as sonoluminescence model, water-splashed problem, and shock waves in bubbly liquids will be considered in the future. Generalization of the algorithm to a solid-liquid-gas three-phase system will be looked at also.

Appendix A. The Riemann Problems. One of the major components of our numerical methods described in Section 3 is the resolution of the Riemann problem in terms of waves at each cell interface. We use a popular approach based on the shock-only approximation of the Riemann solver that ignores the possibility of rarefaction waves, and simply construct a solution in which each pair of the states is connected along Hugoniot locus for a shock (cf. [2, 10, 13]). The application of the approach to the current two-phase (liquid-gas) flow model discussed in Section 2.2 gives an accurate and robust solution procedure that is valid for the type of problems considered in the paper (see Section 4 for numerical results).

To review the basic idea of the method, we consider the Riemann problem normal to the y-axis,

$$\partial_t q + f^{(\partial_x)}(q) = 0, \qquad q(x,y,0) = \begin{cases} q_L & \text{for } x < 0 \\ q_R & \text{for } x > 0, \end{cases}$$

where q and $f^{(\partial_x)}$ are defined as in (2.21). In this approach, the key step is to find the midstate (u_*, p_*) in the u-p plane so that it can connect to (u_L, p_L) by a 1-shock, and to (u_R, p_R) by a 3-shock. It is well-known that this amounts to solving the following nonlinear equation in an iterative manner for the pressure p_*,

$$h(p_*) = u_{*R}(p_*) - u_{*L}(p_*) = 0. \tag{A.1}$$

Here u_{*L} and u_{*R} are the velocities defined by connecting the states along the 1-shock and 3-shock curves, respectively,

$$u_{*L}(p) = u_L - \frac{p - p_L}{W_L(p)}, \qquad u_{*R}(p) = u_R + \frac{p - p_R}{W_R(p)}, \tag{A.2}$$

where W_L and W_R are the corresponding Lagrangian shock speed, for $\iota = L$ or R,

$$W_\iota^2(p) = \begin{cases} \dfrac{p - p_\iota}{\rho_\iota^{-1} - \rho_{*\iota}^{-1}(p)} & \text{if } \mathcal{Z}_\iota = 1 \text{ (liquid phase)} \\[2ex] C_\iota^2 \left[1 + \left(\dfrac{\gamma_\iota + 1}{2\gamma_\iota}\right)\left(\dfrac{p + \mathcal{B}_\iota}{p_\iota + \mathcal{B}_\iota} - 1\right)\right] & \text{if } \mathcal{Z}_\iota \neq 1 \text{ (gas phase)}, \end{cases} \tag{A.3}$$

$C_\iota = \rho_\iota c_\iota$ is the Lagrangian sound speed, and $\rho_{*\iota}$ is the midstate density (see Fig. A.1),

$$\rho_{*\iota}(p) = \begin{cases} \left(\dfrac{p + \mathcal{B}_\iota}{\mathcal{A}_\iota}\right)^{1/\gamma_\iota} & \text{if } \mathcal{Z}_\iota = 1 \text{ (liquid phase)} \\[2ex] \left[\rho_\iota^{-1} - \dfrac{p - p_\iota}{W_\iota^2(p)}\right]^{-1} & \text{if } \mathcal{Z}_\iota \neq 1 \text{ (gas phase)}. \end{cases} \tag{A.4}$$

Note that the above formulae are results derived from the Rankine-Hugoniot jump conditions of Eq. (2.21) (cf. [14, 60, 61]).

When applying a standard root-finding approach such as the secant method to (A.1), we have a 2-step iteration scheme as follows:

$$p_*^{(n+1)} = p_*^{(n)} - \frac{|p_*^{(n)} - p_*^{(n-1)}|}{|u_{*L}^{(n)} - u_{*L}^{(n-1)}| + |u_{*R}^{(n)} - u_{*R}^{(n-1)}|} \left[u_{*R}^{(n)} - u_{*L}^{(n)} \right], \tag{A.5}$$

with $u_{*\iota}^{(n)} = u_{*\iota}\left[p_*^{(n)}\right]$ ($\iota = L$ or R), for $n = 1, 2, \cdots$. With a suitable choice of the starting values $p_*^{(0)}$ and $p_*^{(1)}$, the method (A.5) typically converges to the exact solution p_* at a superlinear rate [27]. For gas dynamics, it is a common practice to set $p_*^{(0)}$ and $p_*^{(1)}$ by

$$\begin{aligned}
p_*^{(0)} &= \frac{p_R C_L + p_L C_R - (u_R - u_L) C_L C_R}{C_L + C_R}, \\
u_{*L}^{(0)} &= u_L - \frac{p_*^{(0)} - p_L}{C_L}, \qquad u_{*R}^{(0)} = u_R + \frac{p_*^{(0)} - p_R}{C_R}, \\
p_*^{(1)} &= \frac{p_R W_L^{(0)} + p_L W_R^{(0)} - (u_R - u_L) W_L^{(0)} W_R^{(0)}}{W_L^{(0)} + W_R^{(0)}},
\end{aligned} \tag{A.6}$$

with $W_\iota^{(0)} = W_\iota\left[p_*^{(0)}\right]$. After a satisfactory convergence of the scheme, we may then compute u_* by

$$u_* = \frac{p_L - p_R + u_L W_L(p_*) + u_R W_R(p_*)}{W_L(p_*) + W_R(p_*)},$$

see [63] for the details.

Fig. A.1 shows a sample solution structure of the Riemann problem mentioned above, where clearly there exist three discontinuities propagation at constant speeds. The propagation speed for each discontinuity is determined by

$$\lambda_1 = u_* - \frac{W_L(p_*)}{\rho_{*L}(p_*)}, \qquad \lambda_2 = u_*, \qquad \lambda_3 = u_* + \frac{W_R(p_*)}{\rho_{*R}(p_*)},$$

and the jumps across each discontinuity are defined as described in §3.

We note that alternatively we may use the 1-step Newton's method for the solution of Eq. (A.1). In this case, the iteration scheme reads

$$p_*^{(n+1)} = p_*^{(n)} - \frac{Y_L^{(n)} Y_R^{(n)}}{Y_L^{(n)} + Y_R^{(n)}} \left[u_{*R}^{(n)} - u_{*L}^{(n)} \right], \quad \text{for } n = 1, 2, \cdots, \tag{A.7}$$

with $Y_\iota^{(n)} = Y_\iota\left[p_*^{(n)}\right]$ and

$$Y_\iota^2(p) = \left| \frac{dp_*}{du_*} \right| = \begin{cases} \dfrac{2C_{*\iota}^2(p)}{W_\iota^2 + C_{*\iota}^2(p)} W_\iota & \text{if } \mathcal{Z}_\iota = 1 \text{ (liquid phase)} \\[2ex] \dfrac{2W_\iota^2}{W_\iota^2 + C_\iota^2} W_\iota & \text{if } \mathcal{Z}_\iota \neq 1 \text{ (gas phase)}, \end{cases} \tag{A.8}$$

where $C_{*\iota}^2 = \rho_{*\iota} c_{*\iota}$. The initial guess of the iteration $p_*^{(0)}$ can be taken the same as in Eq. (A.6) for the secant method. It is known that the rate of convergence of the method is quadratic, when $p_*^{(0)}$ is sufficiently close to p_* [27].

REFERENCES

[1] R. Abgrall. How to prevent pressure oscillations in multicomponent flow calculations: a quasi conservative approach. *J. Comput. Phys.*, 125:150–160, 1996.
[2] D. S. Balsara. Riemann solver for relativistic hydrodynamics. *J. Comput. Phys.*, 114:284–297, 1994.
[3] M. J. Berger and P. Colella. Local adaptive mesh refinement for shock hydrodynamics. *J. Comput. Phys.*, 82:64–84, 1989.
[4] M. J. Berger and R. J. LeVeque. Adaptive mesh refinement using wave-propagation algorithms for hyperbolic systems. *SIAM J. Numer. Anal.*, to appear, 1998.
[5] R. E. Caflisch, M. J. Miksis, G. C. Papanicolaou, and L. Ting. Effective equations for wave propagation in bubbly liquids. *J. Fluid Mech.*, 153:259–273, 1985.
[6] R. E. Caflisch, M. J. Miksis, G. C. Papanicolaou, and L. Ting. Wave propagation in bubbly liquids at finite volume fraction. *J. Fluid Mech.*, 160:1–14, 1985.
[7] E. L. Carstensen and L. L. Foldy. Propagation of sound through a liquid containing bubbles. *J. Acoust. Soc. Am.*, 19:481–501, 1947.
[8] Y. C. Chang, T. Y. Hou, B. Merriman, and S. Osher. A level set formulation of Eulerian interface capturing methods for incompressible fluid flows. *J. Comput. Phys.*, 124:449–464, 1996.
[9] J. D. Cheeke. Single-bubble sonoluminescence: bubble, bubble, toil and trouble. *Can. J. Phys.*, 75:77–96, 1997.
[10] P. Colella. Glimm's method for gas dynamics. *SIAM J. Sci. Stat. Comput.*, 3(1):76–110, 1982.
[11] P. Colella. Multidimensional upwind methods for hyperbolic conservation laws. *J. Comput. Phys.*, 87:171–200, 1990.
[12] P. Colella, R. E. Ferguson, and H. M. Glaz. Multifluid algorithms for Eulerian finite difference methods. *Preprint*, 1994.
[13] P. Colella and H. M. Glaz. Efficient solution algorithms for the Riemann problem for real gases. *J. Comput. Phys.*, 59:264–289, 1985.
[14] C. H. Cooke and T.-J. Chen. On shock capturing for pure wave with general equation of state. *Comm. Pure Appl. Numer. Meth.*, 8:219–233, 1992.
[15] R. Courant and K. O. Friedrichs. *Supersonic Flow and Shock waves*. Wiley-Interscience, New York, 1948.
[16] A. Crespo. Sound and shock waves in liquids containing bubbles. *Phys. Fluids*, 12:2274–2282, 1969.
[17] S. F. Davis. An interface tracking method for hyperbolic systems of conservation laws. *Appl. Numer. Math.*, 10:447–472, 1992.
[18] W. S. Don and C. B. Quillen. Numerical simulation of shock-cylinder interactions: I. resolution. *J. Comput. Phys.*, 122:244–265, 1995.
[19] R. P. Fedkiw, T. Aslam, B. Merriman, and S. Osher. A non-oscillatory Eulerian approach to interfaces in multimaterial flows (the ghost fluid method). *UCLA, CAM Report 98-17*, 1998.
[20] R. P. Fedkiw, X.-D. Liu, and S. Osher. A general technique for eliminating spurious oscillations in conservative schemes for multiphase and multispecies Euler equations. *UCLA, CAM Report 97-27*, 1997.
[21] E. Fermi. *Thermodynamics*. Dover, New York, 1956.
[22] E. Godlewski and P.-A. Raviart. *Numerical Approximation of Hyperbolic Systems of Conservation Laws*. Springer-Verlag, 1996. Applied Mathematical Science 118.
[23] J. Grove. The interaction of shock waves with fluid interfaces. *Adv. in Appl. Math.*, 10:201–227, 1989.
[24] J. Grove and R. Menikoff. The anomalous reflection of a shock wave at a material interface. *J. Fluid. Mech.*, 219:313–336, 1990.
[25] S. Karni. Multicomponent flow calculations by a consistent primitive algorithm. *J. Comput. Phys.*, 112:31–43, 1994.
[26] S. Karni. Hybrid multifluid algorithms. *SIAM J. Sci. Comput.*, 17:1019–1039, 1996.
[27] D. Kincaid and W. Cheney. *Numerical Analysis*. Brooks/Cole, 1990.
[28] R. J. LeVeque. High resolution finite volume methods on arbitrary grids via wave propagation. *J. Comput. Phys.*, 78:36–63, 1988.
[29] R. J. LeVeque. Hyperbolic conservation laws and numerical methods. In *Von Karman Institute for Fluid Dynamics*, 1990. Lecture series on computational fluid dynamics 1990-03.
[30] R. J. LeVeque. *Numerical Methods for Conservation Laws*. Birkhäuser-Verlag, 2 edition, 1992.
[31] R. J. LeVeque. Simplified multi-dimensional flux limiter methods. In M. J. Baines and K. W. Morton, editors, *Numerical Methods for Fluid Dynamics*, pages 175–190. Oxford University

Press, 1993.
[32] R. J. LeVeque. High-resolution conservative algorithms for advection in incompressible flow. *SIAM J. Numer. Anal.*, 33:627–665, 1996.
[33] R. J. LeVeque. Wave propagation algorithms for multi-dimensional hyperbolic systems. *J. Comput. Phys.*, 131:327–353, 1997.
[34] R. J. LeVeque. Balancing source terms and flux gradients in high-resolution godunov methods: The quasi-steady wave propagation algorithm. *J. Comput. Phys.*, to appear, 1998.
[35] R. J. Leveque and D. Bale. Wave propagation method for conservation laws with source terms. In *Proc. 7th Intl. Conf. Hyperbolic Problems*. Birkhäuser-Verlag, 1998. to appear.
[36] R. J. LeVeque and K.-M. Shyue. One-dimensional front tracking based on high resolution wave propagation methods. *SIAM J. Sci. Comput.*, 16:348–377, 1995.
[37] R. J. LeVeque and K.-M. Shyue. Two-dimensional front tracking based on high resolution wave propagation methods. *J. Comput. Phys.*, 123:354–368, 1996.
[38] R. L. LeVeque. CLAWPACK: A software package for solving multi-dimensional conservation laws. In *Proc. 5th Intl. Conf. Hyperbolic Problems*, pages 188–197. World Scientific, 1996.
[39] D. R. Lide. *Handbook of Chemistry and Physics*. CRC Press, 76 edition, 1996.
[40] X.-D. Liu, R. P. Fedkiw, and S. Osher. A quasi-conservative approach to the multiphase Euler equations without spurious pressure oscillations. *UCLA, CAM Report 98-11*, 1998.
[41] G. H. Miller and E. G. Puckett. A high order Godunov method for multiple condensed phases. *J. Comput. Phys.*, 128:134–164, 1996.
[42] H. Nagoya, T. Obara, and K. Takayama. Underwater shock wave propagation and focusing in inhomogeneous media. In R. Brun and L. Z. Dumitrescu, editors, *Proceedings of 19th Intl. Symp. on Shock Waves, Marseille*, pages 439–444. Springer-Verlag, Berlin, 1995.
[43] W. F. Noh and P. Woodward. SLIC (simple line interface calculation). In A. I. van de Vooren and P. J. Zandbergen, editors, *Proc. 5th Intl. Conf. on Numer. Meth. in Fluid Dynamics*. Springer-Verlag, 1976.
[44] L. Noordzij and L. van Wijngaarden. relaxation effects, caused by relative motion, on shock waves in gas-bubble/liquid mixture. *J. Fluid Mech.*, 66:115–143, 1974.
[45] J. E. Pilliod and E. G. Puckett. Second-order volume-of-fluid algorithms for tracking material interfaces. *preprint*, 1993.
[46] J. J. Quirk and S. Karni. On the dynamics of a shock-bubble interaction. *J. Fluid Mech.*, to appear.
[47] W. J. Rider and D. B. Kothe. Reconstructing volume tracking. *J. Comput. Phys.*, 141:112–152, 1998.
[48] P. L. Roe. Approximate Riemann solvers, parameter vector, and difference scheme. *J. Comput. Phys.*, 43:357–372, 1981.
[49] R. Saurel and R. Abgrall. A simple method for compressible multifluid flows. *SIAM J. Sci. Comput.*, to appear, 1998.
[50] R. Saurel and R. Abgrall. Some models and methods for compressible multifluid and multiphase flows. *Preprint*, 1998.
[51] K.-M. Shyue. An adaptive volume-of-fluid approach for compressible multicomponent flows. *In preparation*, 1998.
[52] K.-M. Shyue. An efficient shock-capturing algorithm for compressible multicomponent problems. *J. Comput. Phys.*, 142:208–242, 1998.
[53] K.-M. Shyue. A volume-of-fluid type algorithm for compressible two-phase flows. In *Proc. 7th Intl. Conf. Hyperbolic Problems*. Birkhäuser-Verlag, 1998. to appear.
[54] K.-M. Shyue. *Front Tracking Methods based on Wave Propagation*. Ph.D. thesis, University of Washington, June, 1993 (unpublished).
[55] G. Strang. On the construction and comparison of difference schemes. *SIAM J. Numer. Anal.*, 5:506–517, 1968.
[56] M. Sussman, A. S. Almgren, J. B. Bell, P. Colella, L. H. Howell, and M. L. Welcome. An adaptive level set approach for incompressible two-phase flows. *Preprint*, 1997.
[57] M. Sussman, P. Smereka, and S. Osher. A level set method for computing solutions to incompressible two-phase flow. *J. Comput. Phys.*, 114:146–159, 1994.
[58] P. K. Sweby. High resolution schemes using flux limiters for hyperbolic conservation laws. *SIAM J. Numer Anal.*, 21:995–1011, 1984.
[59] M. J. Tan and S. G. Bankoff. Strong shock waves propagating through a bubbly mixture. *Experiments in Fluids*, 2:159–165, 1984.
[60] H. S. Tang and D. Huang. A second-order accurate capturing scheme for 1D inviscid flows of gas and water with vacuum zones. *J. Comput. Phys.*, 128:301–318, 1996.
[61] E. F. Toro. A fast Riemann solver with constant covolume applied to the random choice method. *Intl. J. Numer. Meth. in Fluids*, 9:1145–1164, 1989.

[62] S. O. Unverdi and G. Tryggvason. A front-tracking method for viscous, incompressible, multi-fluid flows. *J. Comput. Phys.*, 100:25–37, 1992.

[63] B. van Leer. Towards the ultimate conservative difference scheme V. A second order sequel to Godunov's method. *J. Comput. Phys.*, 32:101–136, 1979.

[64] L. van Wijngaarden. One-dimensional flow of liquids containing small gas bubbles. *Ann. Rev. Fluid Mech.*, 4:369–394, 1972.

[65] M. Watanabe and A. Prosperetti. Shock waves in dilute bubbly liquids. *J. Fluid Mech.*, 274:349–381, 1994.

[66] C. C. Wu and P. H. Roberts. A model of sonoluminescence. *Proc. R. Soc. Lon. A*, 445:323–349, 1994.

[67] K. Yamada, H. Nagoya, and K. Takayama. Shock wave reflection and refraction over a two-fluid interface. In R. Brun and L. Z. Dumitrescu, editors, *Proceedings of 19th Intl. Symp. on Shock Waves, Marseille*, pages 299–304. Springer-Verlag, Berlin, 1995.

[68] D. L. Youngs. Time-dependent multi-material flow with large fluid distortion. In K. W. Morton and M. J. Baines, editors, *Numerical Methods for Fluid Dynamics*, pages 273–285. Academic Press, 1982.

[69] Y. B. Zel'dovich and Y. P. Raizer. *Physics of Shock Waves and High-Temperature Hydrodynamic Phenomena*. Academic Press, Vol. I & Vol. II, 1967.

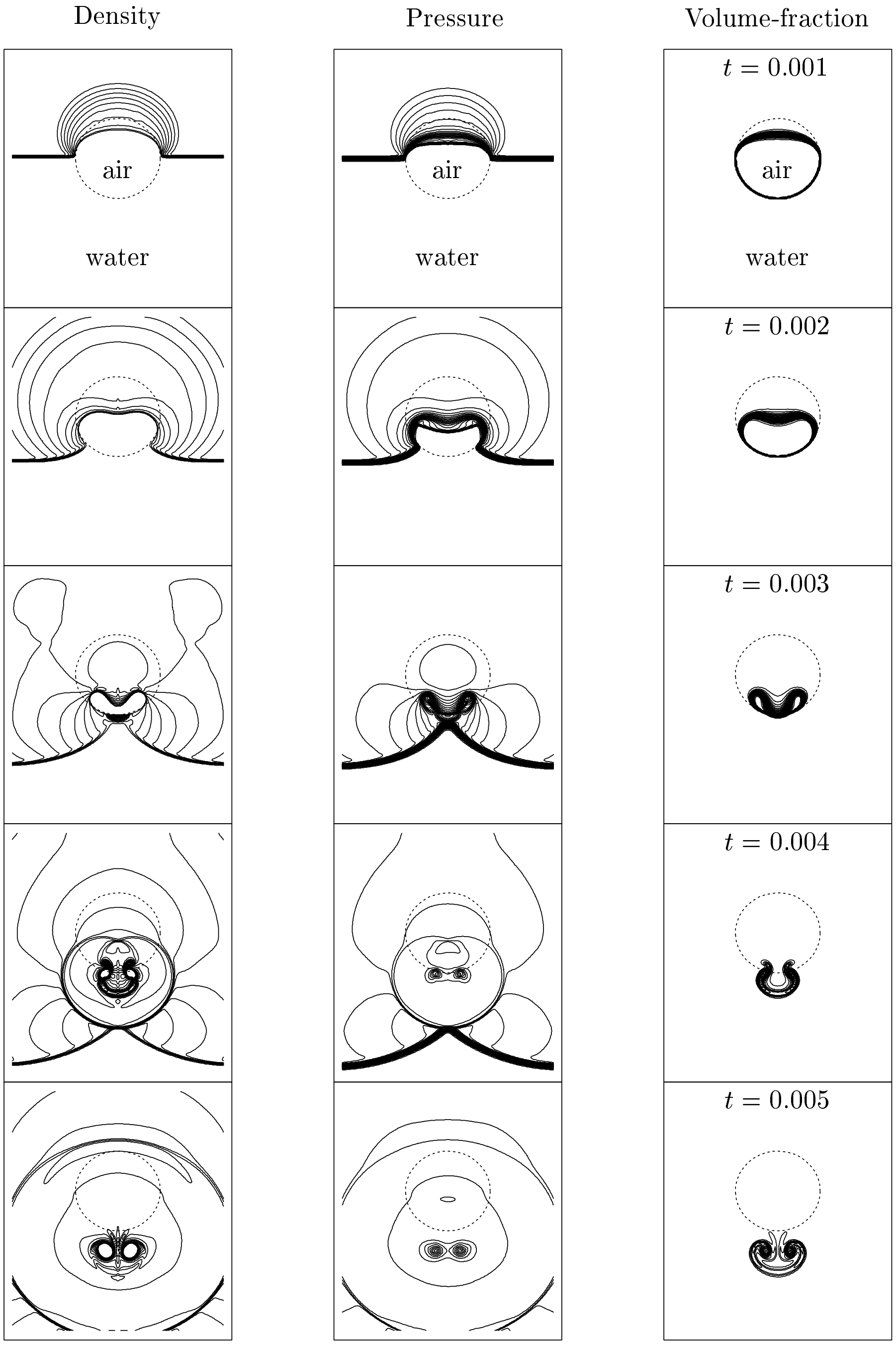

FIG. 4.3. *High-resolution results for a planar Mach* 1.587 *shock wave in water over a bubble of air. Contours of* ρ, p, *and* $\mathcal{Z}$ *are shown at five different times;* $t = (1, 2, 3, 4, 5) \cdot 10^{-3}$ *(*ρ *and* p *are plotted in logarithmic scale). The circular dashed line in all the plots is the initial location of the interface.*

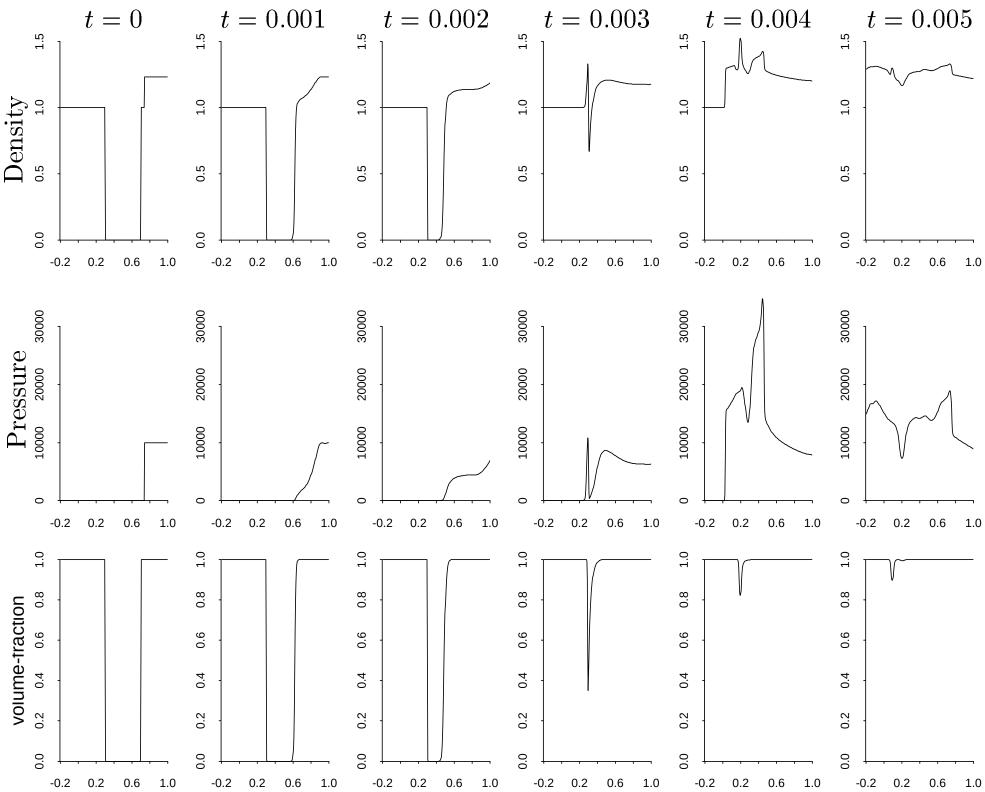

FIG. 4.4. *Cross-sectional plots of the results for the run shown in Fig. 4.3 along line* $x = \frac{1}{2}$.

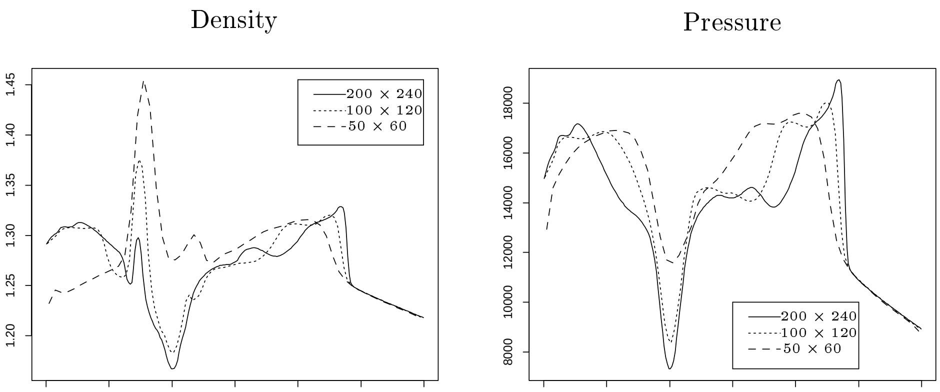

FIG. 4.5. *A convergence study of the density and pressure for a planar Mach* 1.587 *shock wave in water over a bubble of air. The test is performed using a high-resolution version of the method with three different grid systems:* $2^i \cdot (50 \times 60)$, $i = 0, 1, 2$. *Only the cross-sectional solutions along line* $x = \frac{1}{2}$ *at time* $t = 5 \cdot 10^{-3}$ *are presented.*

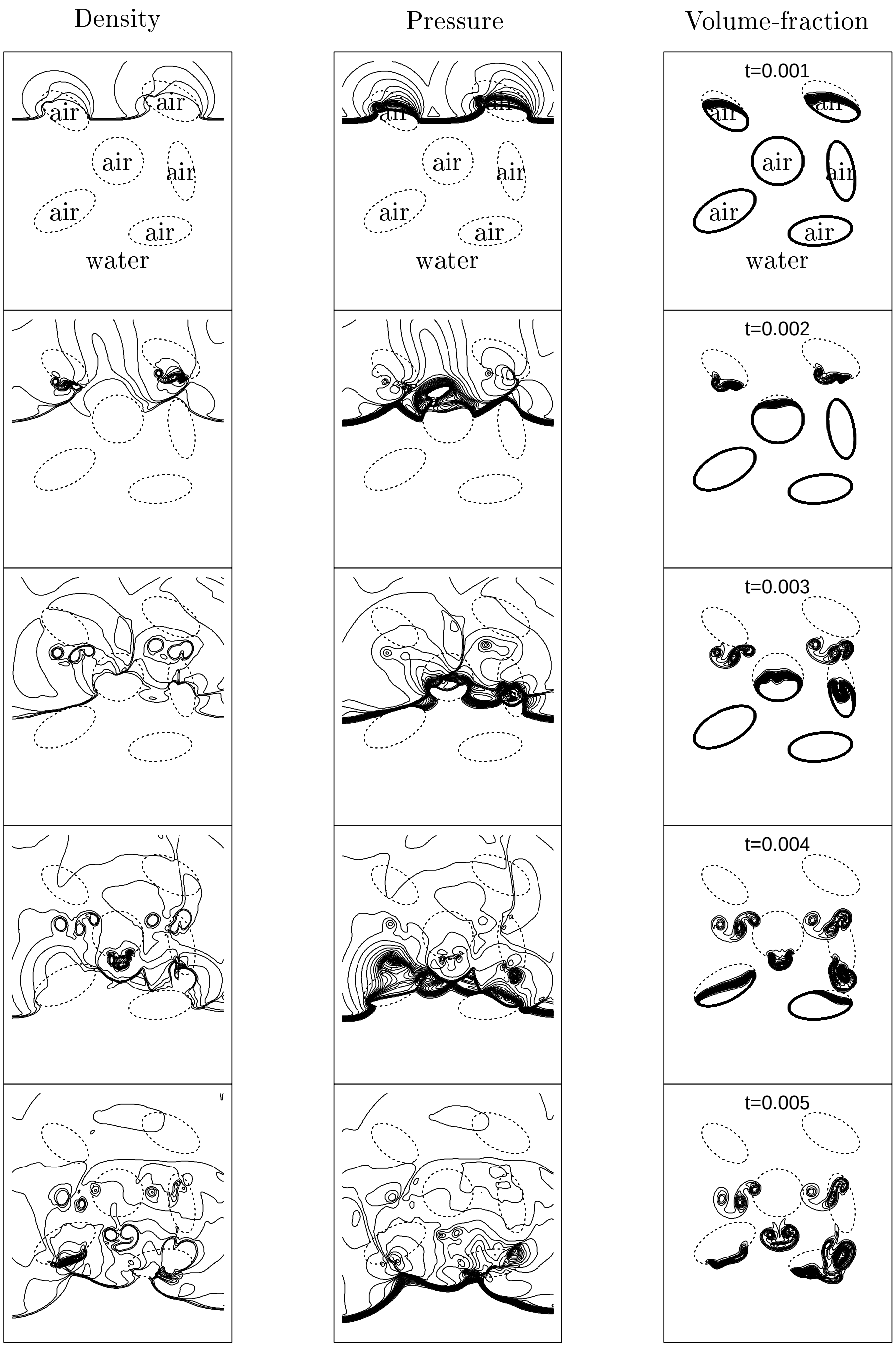

FIG. 4.6. *High-resolution results for a planar Mach* 1.587 *shock wave in water over an array of air bubble. Contours of* ρ, p, *and* $\mathcal{Z}$ *are shown at five different times;* $t = (1, 2, 3, 4, 5) \cdot 10^{-3}$ *(*ρ *and* p *are plotted in logarithmic scale). In all the plots, the different shape of dashed lines are the initial locations of the air bubbles.*

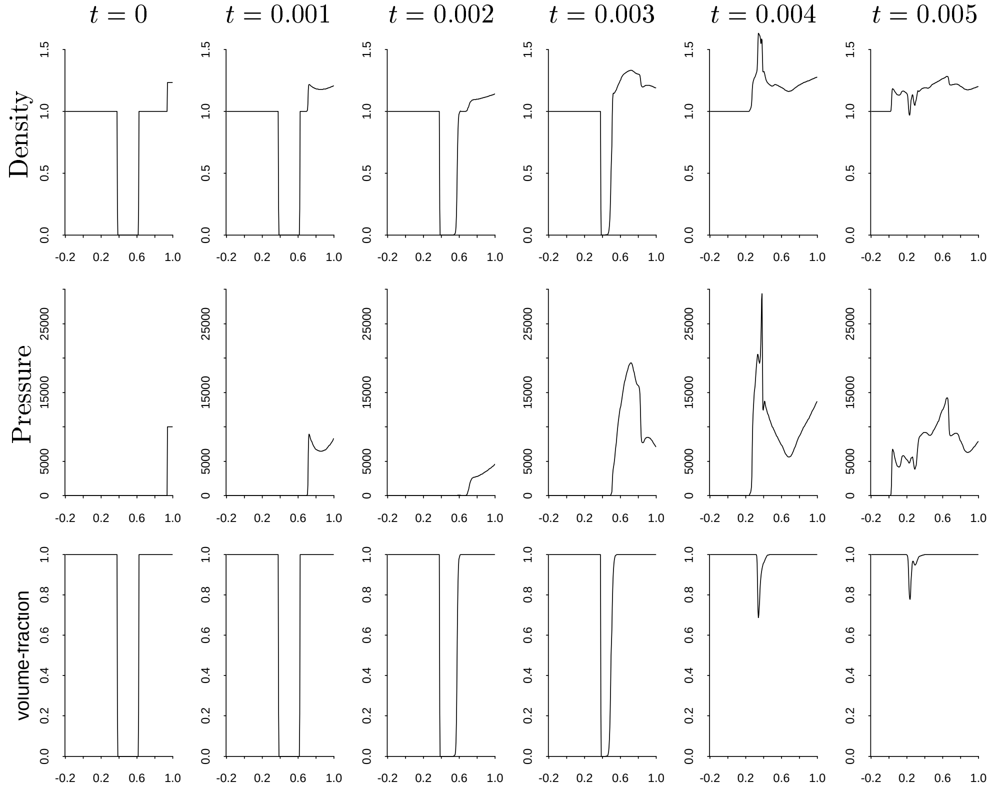

FIG. 4.7. *Cross-sectional plots of the results for the run shown in Fig. 4.6 along line $x = \frac{1}{2}$.*

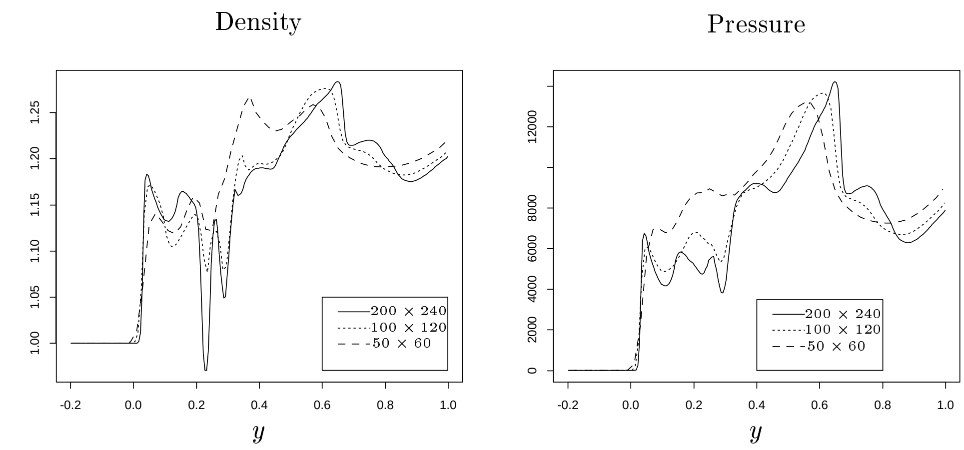

FIG. 4.8. *A convergence study of the density and pressure for a planar Mach 1.587 shock wave in water over an array of air bubbles. The test is performed using a high-resolution version of the method with three different grid systems: $2^i \cdot (50 \times 60)$, $i = 0, 1, 2$. Only the cross-sectional solutions along line $x = \frac{1}{2}$ at time $t = 5 \cdot 10^{-3}$ are presented.*

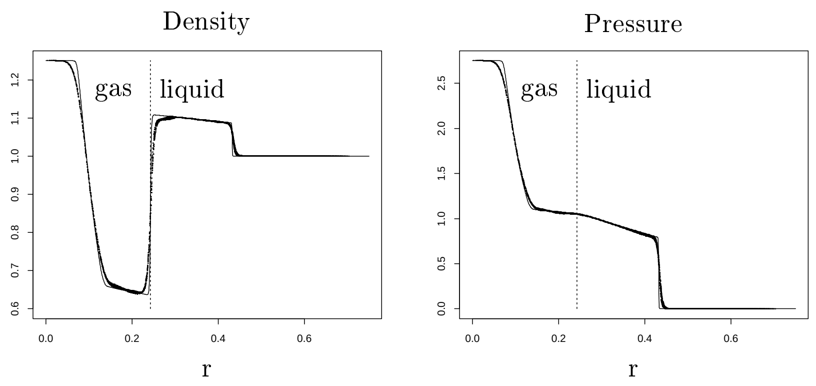

FIG. 5.1. *High-resolution results for a spherically symmetric problem at time $t = 0.07$. Scatter plots of ρ and p with locations measured as a distance from the cell center to the origin. The solid line in the scatter plot is the "true" solution obtained from solving the one-dimensional method with appropriate source terms for the spherical symmetry using the high-resolution method.*

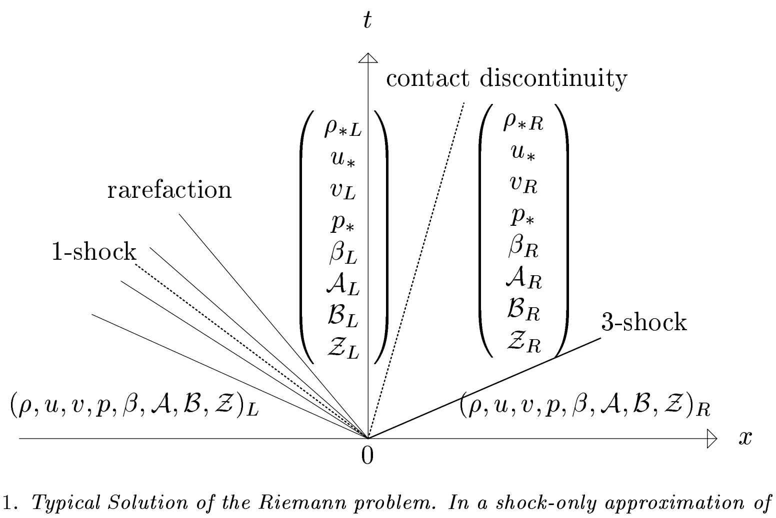

FIG. A.1. *Typical Solution of the Riemann problem. In a shock-only approximation of the exact Riemann solver, the rarefaction wave is replaced by a shock.*